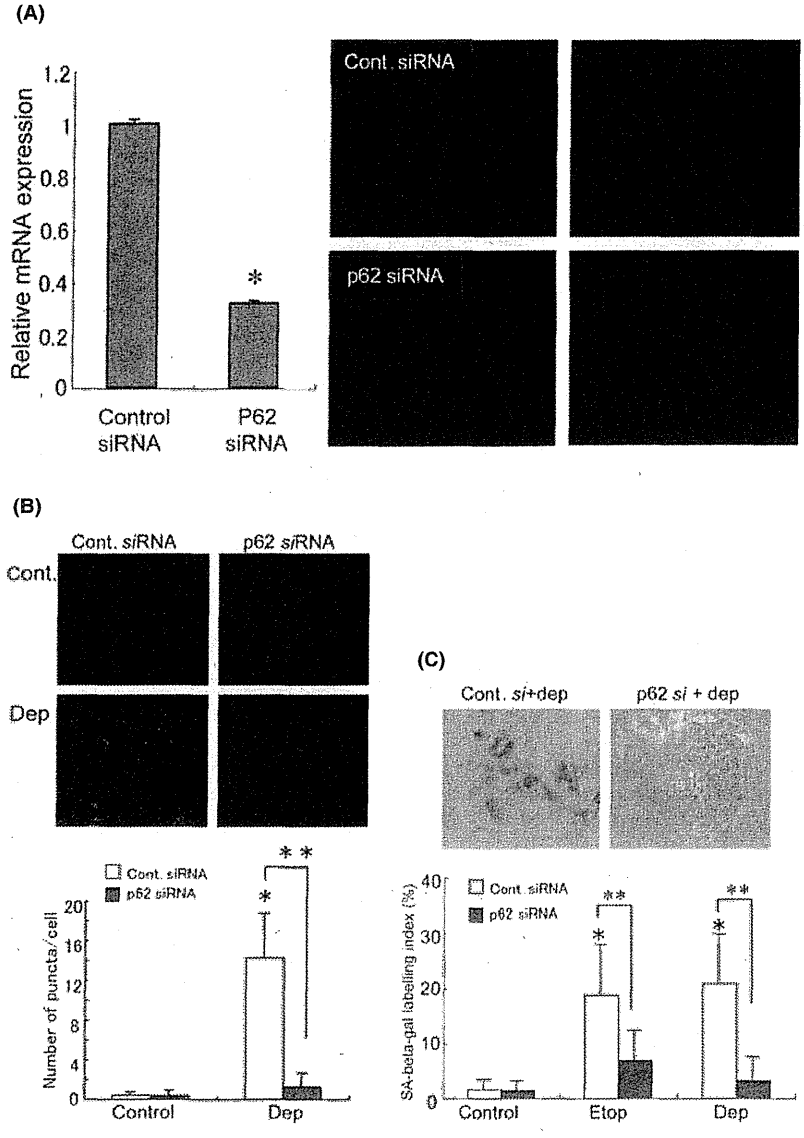

Fig. 7. The knockdown of p62 results in the inhibition of stress-induced autophagy and cellular senescence. (A) Left; the expression of p62mRNA in biliary epithelial cells treated with p62 small interfering RNA (*si*RNA) or control *si*RNA in serum deprivation. p62 mRNA was quantified with real-time PCR and normalized as a ratio using β-actin as the housekeeping gene. Data are expressed as the means ± SD. **P* < 0.01 compared to the control, n = 6 for each group. Right; Immunofluorescent staining for p62 (left column; shown in green) in biliary epithelial cells treated with p62 *si*RNA or control *si*RNA in serum deprivation. Right column, 4′ and 6-diamidino-2-phenylindole (DAPI) nuclear counterstain. Successful knockdown of p62 expression was achieved by the treatment with p62 siRNA. Original magnification, x400. (B) Autophagy was assessed using LC3 puncta formation assay on day1 after a treatment with serum deprivation. LC3-puncta was increased in the cytoplasm of BECs treated with serum deprivation and control *si*RNA, whereas there were few in BECs treated with serum deprivation and p62 *si*RNA. Original magnification, x400. The level of autophagy assessed by LC3 puncta per cell was significantly increased in cells treated with serum deprivation (14.29 ± 4.42), when compared with control (0.42 ± 0.3). The starvation-induced autophagy was significantly inhibited by a treatment with p62 *si*RNA (1.25 ± 1.35), compared with BECs treated with control *si*RNA. (C) Cellular senescence was assessed by senescence-associated β-galactosidase activity (SA-β-gal) on day 4 after a treatment with Etoposide (Etop, 100μM) and serum deprivation (Dep) in combination with p62 siRNA or control siRNA. Percentage of cells positive for SA-β-gal was significantly higher in cells treated with Etoposide (18.8 ± 9.04) and serum deprivation (20.9 ± 8.95), when compared with control without treatment (1.68 ± 1.78). Percentage of cells positive for SA-β-gal significantly decreased by a treatment with p62 siRNA (dark columns; Etop, 6.91 ± 5.42; Dep, 3.24 ± 4.25). Data are expressed as mean ± SD. **P* < 0.01 compared to control, ***P* < 0.01.

References

1. Mizushima N, Levine B, Cuervo AM, Klionsky DJ. Autophagy fights disease through cellular self-digestion. *Nature* 2008; **451**: 1069–75.
2. Ohsumi Y. Molecular dissection of autophagy: two ubiquitin-like systems. *Nat Rev Mol Cell Biol* 2001; **2**: 211–6.
3. Young AR, Narita M, Ferreira M, *et al.* Autophagy mediates the mitotic senescence transition. *Genes Dev* 2009; **23**: 798–803.
4. White E, Lowe SW. Eating to exit: autophagy-enabled senescence revealed. *Genes Dev* 2009; **23**: 784–7.
5. Levine B, Kroemer G. Autophagy in the pathogenesis of disease. *Cell* 2008; **132**: 27–42.
6. Yin XM, Ding WX, Gao W. Autophagy in the liver. *Hepatology* 2008; **47**: 1773–85.
7. Teckman JH, An JK, Blomenkamp K, Schmidt B, Perlmutter D. Mitochondrial autophagy and injury in the liver in alpha 1-antitrypsin deficiency. *Am J Physiol Gastrointest Liver Physiol* 2004; **286**: G851–62.
8. Wang Y, Singh R, Xiang Y, Czaja M J. Macroautophagy and chaperone-mediated autophagy are required for hepatocyte resistance to oxidant stress. *Hepatology* 2010; **52**: 266–77.
9. Singh R, Kaushik S, Wang Y, *et al.* Autophagy regulates lipid metabolism. *Nature* 2009; **458**: 1131–5.
10. Komoatsu M, Kurokawa H, Waguri S, *et al.* The selective autophagy substrate p62 activates the stress responsive transcription factor Nrf2 through inactivation of Keap1. *Nat Cell Biol* 2010; **12**: 213–23.
11. Sasaki M, Miyakoshi M, Sato Y, Nakanuma Y. Autophagy mediates the process of cellular senescence characterizing bile duct damages in primary biliary cirrhosis. *Lab Invest* 2010; **90**: 835–43.
12. Mathew R, Karp CM, Beaudoin B, *et al.* Autophagy suppresses tumorigenesis through elimination of p62. *Cell* 2009; **137**: 1062–75.
13. Bartkova J, Rezaei N, Liontos M, *et al.* Oncogene-induced senescence is part of the tumorigenesis barrier imposed by DNA damage checkpoints. *Nature* 2006; **444**: 633–7.
14. Acosta JC, O'loghlen A, Banito A, *et al.* Chemokine signaling via the CXCR2 receptor reinforces senescence. *Cell* 2008; **133**: 1006–18.
15. Kuilman T, Michaloglou C, Vredeveld LC, *et al.* Oncogene-induced senescence relayed by an interleukin-dependent inflammatory network. *Cell* 2008; **133**: 1019–31.
16. Wajapeyee N, Serra RW, Zhu X, Mahalingam M, Green MR. Oncogenic BRAF induces senescence and apoptosis through pathways mediated by the secreted protein IGFBP7. *Cell* 2008; **132**: 363–74.
17. Portmann B, Nakanuma Y. Diseases of the bile ducts. In: Burt A, BC P, LD F, eds. *Pathology of the Liver*. 5th edn. London: Churchill Livingstone, 2007; 517–81.
18. Kaplan MM, Gershwin ME. Primary biliary cirrhosis. *N Engl J Med* 2005; **353**: 1261–73.
19. Lindor KD, Gershwin ME, Poupon R, *et al.* Primary biliary cirrhosis. *Hepatology* 2009; **50**: 291–308.
20. Nakanuma Y, Ohta G. Histometric and serial section observations of the intrahepatic bile ducts in primary biliary cirrhosis. *Gastroenterology* 1979; **76**: 1326–32.
21. Fussey S, Guest J, James O, Bassendine M, Yeaman S. Identification and analysis of the major M2 autoantigens in primary biliary cirrhosis. *Proc Natl Acad Sci USA* 1988; **85**: 8654–8.
22. Kita H, Matsumura S, He XS, *et al.* Quantitative and functional analysis of PDC-E2-specific autoreactive cytotoxic T lymphocytes in primary biliary cirrhosis. *J Clin Invest* 2002; **109**: 1231–40.
23. Shimoda S, Van de Water J, Ansari A, *et al.* Identification and precursor frequency analysis of a common T cell epitope motif in mitochondrial autoantigens in primary biliary cirrhosis. *J Clin Invest* 1998; **102**: 1831–40.
24. Sasaki M, Ikeda H, Haga H, Manabe T, Nakanuma Y. Frequent cellular senescence in small bile ducts in primary biliary cirrhosis: a possible role in bile duct loss. *J Pathol* 2005; **205**: 451–9.
25. Sasaki M, Ikeda H, Sato Y, Nakanuma Y. Decreased expression of Bmi1 is closely associated with cellular senescence in small bile ducts in primary biliary cirrhosis. *Am J Pathol* 2006; **169**: 831–45.
26. Sasaki M, Ikeda H, Yamaguchi J, Nakada S, Nakanuma Y. Telomere shortening in the damaged small bile ducts in primary biliary cirrhosis reflects ongoing cellular senescence. *Hepatology* 2008; **48**: 186–95.
27. Sasaki M, Ikeda H, Nakanuma Y. Activation of ATM signaling pathway is involved in oxidative stress-induced expression of mito-inhibitory p21(WAF1/Cip1) in chronic non-suppurative destructive cholangitis in primary biliary cirrhosis: an immunohistochemical study. *J Autoimmun* 2008; **31**: 73–8.
28. Lamark T, Kirkin V, Dikic I, Johansen T. NBR1 and p62 as cargo receptors for selective autophagy of ubiquitinated targets. *Cell Cycle* 2009; **8**: 1986–90.
29. Ichimura Y, Kumanomidou T, Sou YS, *et al.* Structural basis for sorting mechanism of p62 in selective autophagy. *J Biol Chem* 2008; **283**: 22847–57.
30. Bjorkoy G, Lamark T, Brech A, *et al.* p62/SQSTM1 forms protein aggregates degraded by autophagy and has a protective effect on huntingtin-induced cell death. *J Cell Biol* 2005; **171**: 603–14.
31. Pankiv S, Clausen T H, Lamark T, *et al.* p62/SQSTM1 binds directly to Atg8/LC3 to facilitate degradation of ubiquitinated protein aggregates by autophagy. *J Biol Chem* 2007; **282**: 24131–45.
32. Kuusisto E, Salminen A, Alafuzoff I. Ubiquitin-binding protein p62 is present in neuronal and glial inclusions in human tauopathies and synucleinopathies. *Neuroreport* 2001; **12**: 2085–90.
33. Stumptner C, Fuchsbichler A, Heid H, Zatloukal K, Denk H. Mallory body – a disease-associated type of sequestosome. *Hepatology* 2002; **35**: 1053–62.
34. Zatloukal K, Stumptner C, Fuchsbichler A, *et al.* p62 Is a common component of cytoplasmic inclusions in protein aggregation diseases. *Am J Pathol* 2002; **160**: 255–63.
35. Komatsu M, Waguri S, Koike M, *et al.* Homeostatic levels of p62 control cytoplasmic inclusion body formation in autophagy-deficient mice. *Cell* 2007; **131**: 1149–63.
36. Nezis IP, Simonsen A, Sagona AP, *et al.* Ref(2)P, the Drosophila melanogaster homologue of mammalian p62, is required for the formation of protein aggregates in adult brain. *J Cell Biol* 2008; **180**: 1065–71.
37. Monick MM, Powers LS, Walters K, *et al.* Identification of an autophagy defect in smokers' alveolar macrophages. *J Immunol* 2010; **185**: 5425–35.

38. Nakanuma Y, Sasaki M. Expression of blood-group-related antigens in the intrahepatic biliary tree and hepatocytes in normal livers and various hepatobiliary diseases. *Hepatology* 1989; **10**: 174–8.
39. Roskams TA, Theise ND, Balabaud C, *et al.* Nomenclature of the finer branches of the biliary tree: canals, ductules, and ductular reactions in human livers. *Hepatology* 2004; **39**: 1739–45.
40. Desmet V, Gerber M, Hoofnagle J, Manns M, Scheuer P. Classification of chronic hepatitis: diagnosis, grading and staging. *Hepatology* 1994; **19**: 1513–20.
41. Nakanuma Y, Kono N, Ohta G, Kato Y, Kobayashi K. Ultrastructural changes of bile duct epithelium in primary biliary cirrhosis in relation to progression of bile duct loss. *Virchows Arch A Pathol Anat Histopathol* 1982; **398**: 149–61.
42. Katayanagi K, Kono N, Nakanuma Y. Isolation, culture and characterization of biliary epithelial cells from different anatomical levels of the intrahepatic and extrahepatic biliary tree from a mouse. *Liver* 1998; **18**: 90–8.
43. Seglen PO, Gordon P B. 3-Methyladenine: specific inhibitor of autophagic/lysosomal protein degradation in isolated rat hepatocytes. *Proc Natl Acad Sci U S A* 1982; **79**: 1889–92.
44. Boya P, Gonzalez-Polo R A, Casares N, *et al.* Inhibition of macroautophagy triggers apoptosis. *Mol Cell Biol* 2005; **25**: 1025–40.
45. Sasaki M, Van de Water J, Kenny TP, *et al.* Immunoglobulin gene usage and immunohistochemical characteristics of human monoclonal antibodies to the mitochondrial autoantigens of primary biliary cirrhosis induced in the XenoMouse. *Hepatology* 2001; **34**(4 Pt 1): 631–7.
46. Mizushima N, Yoshimori T, Levine B. Methods in mammalian autophagy research. *Cell* 2010; **140**: 313–26.
47. Dimri G P, Lee X, Basile G, *et al.* A biomarker that identifies senescent human cells in culture and in aging skin *in vivo*. *Proc Natl Acad Sci U S A* 1995; **92**: 9363–7.
48. Stein G H, Drullinger LF, Soulard A, Dulic V. Differential roles for cyclin-dependent kinase inhibitors p21 and p16 in the mechanisms of senescence and differentiation in human fibroblasts. *Mol Cell Biol* 1999; **19**: 2109–17.
49. Takeuchi S, Takahashi A, Motoi N, *et al.* Intrinsic cooperation between p16INK4a and p21Waf1/Cip1 in the onset of cellular senescence and tumor suppression *in vivo*. *Cancer Res* 2010; **70**: 9381–90.
50. Nogalska A, D'agostino C, Terracciano C, Engel WK, Askanas V. Impaired autophagy in sporadic inclusion-body myositis and in endoplasmic reticulum stress-provoked cultured human muscle fibers. *Am J Pathol* 2010; **177**: 1377–87.
51. Chedid A, Spellberg MA, Debeer RA. Ultrastructural aspects of primary biliary cirrhosis and other types of cholestatic liver disease. *Gastroenterology* 1974; **67**: 858–69.
52. Madeo F, Tavernarakis N, Kroemer G. Can autophagy promote longevity? *Nat Cell Biol* 2010; **12**: 842–6.
53. Narita M, Young AR, Arakawa S, *et al.* Spatial coupling of mTOR and autophagy augments secretory phenotypes. *Science* 2011; **332**: 966–70.

Supporting information

Additional Supporting Information may be found in the online version of this article:

Fig. S1. Apoptosis was assessed using the ssDNA apoptosis ELISA kit (Millipore, Billerica, MA, USA) according to the manufacturer's protocol on day 4 after a treatment with serum deprivation (Dep). It was found that the serum deprivation for 4 days tended to induce a slight increase of apoptosis (relative apoptosis index; 0.218 ± 0.033), compared to control (0.194 ± 0.031), but there was no significant difference ($P > 0.05$).

Please note: Wiley-Blackwell are not responsible for the content or functionality of any supporting materials supplied by the authors. Any queries (other than missing material) should be directed to the corresponding author for the article.

Cyst-Forming Intraductal Papillary Neoplasm of the Bile Ducts: Description of Imaging and Pathologic Aspects

Jae Hoon Lim[1]
Yoh Zen[2]
Kee Taek Jang[3]
Young Kon Kim[1]
Yasuni Nakanuma[4]

OBJECTIVE. Intraductal papillary neoplasm (IPN) of the bile duct is a newly described pathologic entity characterized by the presence of intraluminal tumors, which sometimes produce a large amount of mucin and form a cystic tumor. Cystic IPN of the bile duct is different from biliary cystadenoma or cystadenocarcinoma in that the former produces intraductal microscopic and macroscopic papillary tumors without ovarian-like stroma, whereas the latter produce a mucin-containing septate cystic tumor without communication with bile duct and with ovarian-like stroma in the cyst wall. The purpose of this study was to evaluate the potential relationships between cyst-forming IPNs of the bile duct and peribiliary glands and also intraductal papillary mucinous neoplasms of the pancreas.

MATERIALS AND METHODS. From a cohort of 87 patients with surgically resected and pathologically proved IPN of the bile duct, 12 patients with cystic IPN of the bile duct who underwent CT (n = 12), MRCP (n = 3), ultrasound (n = 3), and ERCP (n = 4) were included. Imaging findings were evaluated for the relationship of cystic tumors to the bile ducts; in particular, a diverticulum-like appearance was considered as suggestive of the peribiliary gland origin. Pathologic examination was conducted, and both gross and microscopic findings were recorded.

RESULTS. Radiologic examination revealed aneurysm-like dilatation of the involved bile ducts in five patients and intrahepatic biliary cystic tumor in two patients. Interestingly, the remaining five patients had diverticulum-like cystic tumor with or without communication; one patient had a cystic tumor laterally attached to the extrahepatic bile duct. Histopathologically, cystic tumors are lined by atypical biliary epithelium showing intracystic papillary proliferation, with an appearance similar to that of pancreatic intraductal papillary mucinous neoplasm.

CONCLUSION. This study suggests that cyst-forming IPN of the bile duct may be a biliary counterpart to pancreatic intraductal papillary mucinous neoplasm. In particular, at least some of the tumors seem to arise from peribiliary glands, and these cases might be a counterpart to branch-duct intraductal papillary mucinous neoplasm of the pancreas, given the histologic similarity between peribiliary glands and pancreatic branch ducts.

Keywords: biliary cystic neoplasm, biliary papillomatosis, cholangiocarcinoma, intraductal bile duct papillary neoplasm, intraductal papillary mucinous neoplasm

DOI:10.2214/AJR.10.6363

Received December 22, 2010; accepted after revision April 27, 2011.

[1]Department of Radiology and Center for Imaging Science, Samsung Medical Center, Sungkyunkwan University School of Medicine, 50 Ilwon-dong, Gangnam-gu, Seoul 135-710, Republic of Korea. Address correspondence to J. H. Lim (jhlim@skku.edu).

[2]Department of Pathology, Institute of Liver Studies, King's College Hospital, London, United Kingdom.

[3]Department of Pathology, Samsung Medical Center, Sungkyunkwan University School of Medicine, Seoul, Republic of Korea.

[4]Department of Pathology, Kanazawa University Graduate School of Medicine, Kanazawa, Japan.

AJR 2011; 197:1111–1120

0361–803X/11/1975–1111

Biliary cystic tumors mostly refer to biliary cystadenomas or cystadenocarcinomas that form a unilocular or septate multilocular cystic cavity containing mucin, and mural nodules or excrescences may also be observed along the capsular wall [1–3]. Neoplastic biliary epithelial cells grow on the luminal surface and not infrequently present with papillary growth with fine vascular cores. Communication between these cystic tumors and the bile duct lumen are usually absent. The cystic tumors show ovarian-like stroma in the cyst wall. These cystic tumors are newly classified as mucinous cystic neoplasms in the World Health Organization classification of biliary tumors [4].

Recently, "intraductal papillary neoplasm (IPN) of the bile duct" was proposed as the term to describe the biliary tumor characterized by the presence of intraluminal papillary tumors with fine fibrovascular cores in the dilated bile ducts. Some cases have shown invasion onto the bile duct wall [5–8]. Not infrequently, excessive mucin is produced by neoplastic cells, and the affected bile duct is filled with mucin and shows tubular or cystic luminal dilatation [9]. The disease, which is distinctly different from mucinous cystic neoplasms, is newly recognized in the World Health Organization classification of biliary neoplasms [4].

Although most cases of IPN of the bile duct show tubular or fusiform dilatation of

TABLE 1: Clinical, Radiologic, Surgical, and Pathologic Findings in 12 Patients With Cystic Intraductal Papillary Mucinous Tumor of the Bile Ducts

Patient No.	Age (y)	Sex	Clinical Findings	Imaging Findings of Cystic Tumor	Location	Bile Duct Dilatation	Mucin in the Downstream Bile Ducts	Gross Pathologic and Surgical Findings	Histopathologic Diagnosis	Tumor Growing Pattern	Survival After Surgery
1	71	Female	Right upper abdominal pain	Three loculated cysts (8 × 5 × 4 cm) containing fungating tumors (ultrasound, CT, and MRCP)	Right lobe	Right lobe and extrahepatic	Present (ERCP)	Multiloculated cystic mass containing multiple fungating masses and mucin	Papillary adenocarcinoma, mucin producing, intestinal phenotype	Fungating papillary tumor in the aneurysmally dilated bile duct	Died 2 years later of malignancy
2	53	Female	Intermittent abdominal pain for 4 months and recent dyspnea and fever	Multiloculated cystic lesion with papillary excrescences (13 × 12 × 13 cm) (CT)	Left and caudate lobe	Left lobe and caudate lobe and extrahepatic	Present (ERCP)	Cystic tumor containing mucopurulent fluid and fragile tumor debris; rupture and cardiac tamponade	Papillary adenocarcinoma, mucin producing (superimposed infection), pancreatobiliary phenotype	Multiple fungating papillary tumors in the aneurysmally dilated bile duct; cyst rupture and peritoneal implants	Died of cardiac tamponade
3	53	Male	Epigastric pain and fever	Cystic lesion containing fluid and fungating tumors (9 × 5 × 5 cm) (CT and ultrasound)	Left lobe	Left and right lobe and extrahepatic	Present (ERCP)	Cystic tumor containing multiple fungating papillary tumor (intraductal stone combined) and mucin (Fig. 1)	Papillary adenocarcinoma, mucin producing, pancreatobiliary phenotype	Fungating papillary tumor in the aneurysmally dilated bile duct	Died 4 years later of malignancy
4	63	Male	Epigastric discomfort	Cystic tumor filled with fluid and solid tumors (5 × 5 × 3 cm) (CT)	Left lobe	Left lobe	Absent	Cystic tumor containing fungating tumor and mucin	Papillary adenocarcinoma, mucin producing, intestinal phenotype	Fungating papillary tumor in the aneurysmally dilated bile duct	Lost to follow-up
5	76	Male	No symptom; incidentally found cystic liver mass	Single cyst (11 × 9 cm), multiple excrescences (CT)	Left lobe	Absent	Absent	Cystic tumor containing thick trabeculae of tumor and mucin	Papillary intraductal adenocarcinoma, mucin producing, intestinal phenotype	Multiple papillary tumors, eccentrically located in the large cyst	Lost to follow-up
6	51	Male	Abdominal pain and vomiting	Single cyst (17 × 16 cm), 3 discrete masses (1–2 cm) attached to the cyst wall (CT and ultrasound)	Left lobe	Absent	Absent	Cystic tumor containing three mural nodules and mucin	Papillary intraductal adenocarcinoma, mucin producing, oncocytic phenotype	Three small discrete papillary tumors attached to the cyst wall	Surviving for 7 years after surgery
7	67	Female	General weakness and anorexia	Cystic and fusiform dilatation of right and left hepatic ducts and extrahepatic ducts (8 × 5 × 4 cm) containing multiple scattered papillary excrescences (CT and MRI)	Right and left hepatic ducts	Right and left lobe and extrahepatic duct	Present (Endoscopy)	Aneurysmally dilated multiple bile ducts studded with innumerable papillary tumors inside	Intraductal papillary tumor (carcinoma), oncocytic phenotype	Multiple excrescences of papillary tumors in aneurysmally dilated right hepatic duct and branches and common hepatic duct	Surviving for 3 years after surgery
8	49	Female	Liver mass on ultrasound examination	Aneurysmally dilated left hepatic duct (4 × 4 × 3.5 cm) containing a solid mass; rupture of proximal bile ducts and multiple lobulated mucin collection at liver surface (CT)	Left lobe lateral segment	Left lobe and caudate lobe and extrahepatic duct	Present (ERCP)	Cystic dilatation of left duct with papillary tumor inside; multiloculated mucin collections at liver surface	Intraductal papillary tumor (carcinoma) with focal invasion, intestinal phenotype	Multiple papillary tumors studded in the cystically dilated left hepatic duct	Surviving for 6 years after surgery

(Table 1 continues on next page)

TABLE 1: Clinical, Radiologic, Surgical, and Pathologic Findings in 12 Patients With Cystic Intraductal Papillary Mucinous Tumor of the Bile Ducts (continued)

Patient No.	Age (y)	Sex	Clinical Findings	Imaging Findings of Cystic Tumor	Location	Bile Duct Dilatation	Mucin in the Downstream Bile Ducts	Gross Pathologic and Surgical Findings	Histopathologic Diagnosis	Tumor Growing Pattern	Survival After Surgery
9	46	Male	Cystic liver tumor on ultrasound examination	Multiloculated cystic mass (4.5 × 4 × 4 cm) with multiple excrescences inside and thin septae (CT)	Left lobe, lateral segment	Absent	Absent	Multiloculated cystic tumor, multiple excrescences inside (Fig. 2)	Intraductal papillary neoplasm (carcinoma) confined to duct wall pancreatobiliary phenotype	Multiple papillary tumors in each chamber	Surviving for 2 years after surgery
10	65	Female	Epigastric discomfort	Unilocular cyst bulging out from liver (10 × 8 × 6 cm) containing myriad small papillary projections (CT)	Caudate lobe	Absent	Absent	Large cystic tumor of caudate lobe containing friable fine papillary tumors and mucin (Fig. 3)	Intraductal papillary tumor (carcinoma) pancreatobiliary phenotype	Myriad frondlike tiny papillary tumors projecting into cystic mass like stalactites	Died 2 years later of malignancy
11	56	Female	Cystic lesion on ultrasound examination	Unilocular cyst (4 × 3.5 × 3.5 cm) containing a solid nodule attached to cyst wall (ultrasound and CT)	Extrahepatic duct	Absent	Absent	Cystic tumor attached to common hepatic duct with a tumor nodule inside	Intraductal papillary neoplasm (carcinoma) confined to the duct wall, oncocytic phenotype	Single nodular tumor attached to cyst wall	Surviving for 4 years after surgery
12	62	Female	Jaundice	Multiloculated cyst associated with dilated right and left hepatic ducts (5.5 × 5 × 4.5 cm) (CT and MRI)	Right and left bile ducts	Mild dilatation of proximal ducts	Absent	Cystically dilated right and left ducts, filled with mucin	Intraductal papillary neoplasm (invasive carcinoma), pancreatobiliary phenotype	No gross tumor; tumor cells lining the cyst wall	Surviving for 3 years after surgery

the involved bile duct, several cases have shown cystic dilatation of the affected bile ducts, appearing as a vascular aneurysm or diverticulum [9, 10]. The latter type has been proposed to be cyst-forming IPN of the bile duct, and in fact, there have been sporadic reports so far [10–14]. This cystic type of neoplasm lacks ovarian-like stroma in the cyst wall and usually shows luminal communication with the bile duct, thus differing from biliary mucinous cystic neoplasms. Such cases resemble cyst-forming branch-duct intraductal papillary mucinous neoplasms of the pancreas and can be regarded as biliary counterparts of pancreatic intraductal papillary mucinous neoplasms [15–17].

Recently, biologic similarities between the biliary and pancreatic ductal systems have attracted attention [18]. Similar tumors, including IPNs, intraepithelial neoplasms, and mucinous cystic neoplasms, can arise in biliary and pancreatic ducts [18–21]. Both organs are derived from the ventral endoderm of the foregut. Extrahepatic or hilar bile ducts and main pancreatic ducts are histologically similar, as evidenced by a lining of flat columnar epithelium constantly expressing keratins 7 and 19. It is still uncertain which structure of the biliary system corresponds to branch ducts of the pancreas. Because peribiliary glands sometimes show pancreatic acinar cell metaplasia, their conduits may correspond to branch or smaller pancreatic ducts [18].

We have recorded 12 cases of cyst-forming IPN of the bile duct over a 15-year period. In this study, we examined clinicopathologic features of these cases, particularly their imaging features. The goal of this study is to reveal whether any cases have evidence suggestive of the peribiliary gland origin and whether cyst-forming IPNs of the bile duct may correspond to branch-duct intraductal papillary mucinous neoplasms of the pancreas.

Materials and Methods

This retrospective study was approved by the institutional review board, and informed consent was waived. A review of the pathology database of Samsung Medical Center over a 15-year period (1995–2009) identified 12 cases of cyst-forming IPN of the bile duct. During the same period, 1127 patients with cholangiocarcinoma underwent surgical resection, including 87 patients with IPN of the bile duct; the 12 patients described here were among the 87 patients (14% [12/87]). Cyst-forming IPN of the bile duct is defined as a gross cystic dilatation of tumor-bearing bile ducts and balloonlike or diverticulum-like dilatation of the bile duct in which there are tumor nodules or excrescences. There were five men and seven women (age range, 46–76 years; average age, 59 years). Demographic features, clinical presentation, tumor location, and treatment are shown in Table 1. Because the disease is a newly recognized disease entity showing interesting pathologic and imaging features, some of the cases were included in previous publications (patient 2 [22], patients 3 and 4 [9], patient 7 [10], and patients 1–7 [23]).

Imaging Methods

CT—CT was performed on all patients using commercially available helical or MDCT scanners. CT techniques were not standardized because of the 15-year span of the study. Unenhanced and contrast-enhanced CT was performed using commercially available single-detector (n = 4), MDCT (n = 3), and 16-MDCT or higher (n = 5) CT scanners. Unenhanced CT was performed using 7.5–10-mm thickness and 7.5–10.0-mm intervals. Using a bolus-triggered technique, arterial phase scanning was started at 30–45 seconds after the start of injection of 120 mL of nonionic iodinated contrast material through the antecubital vein at 4 mL/s, using 0.625–3.0-mm slice thickness and 0.625–3.0-mm intervals. The portal phase of scanning began 70 seconds after the start of contrast material injection with 5-mm slice thickness and 5-mm intervals.

Ultrasound—In three patients, routine transabdominal hepatobiliary and pancreas ultrasound were performed in the supine and right anterior oblique positions. All scans were performed with commercially available high-end ultrasound units with 2–5-MHz probes.

MRCP—MRCP was performed in three patients using commercially available 1.5 T scanners with phased-array multicoil systems. Coronal single-projection images

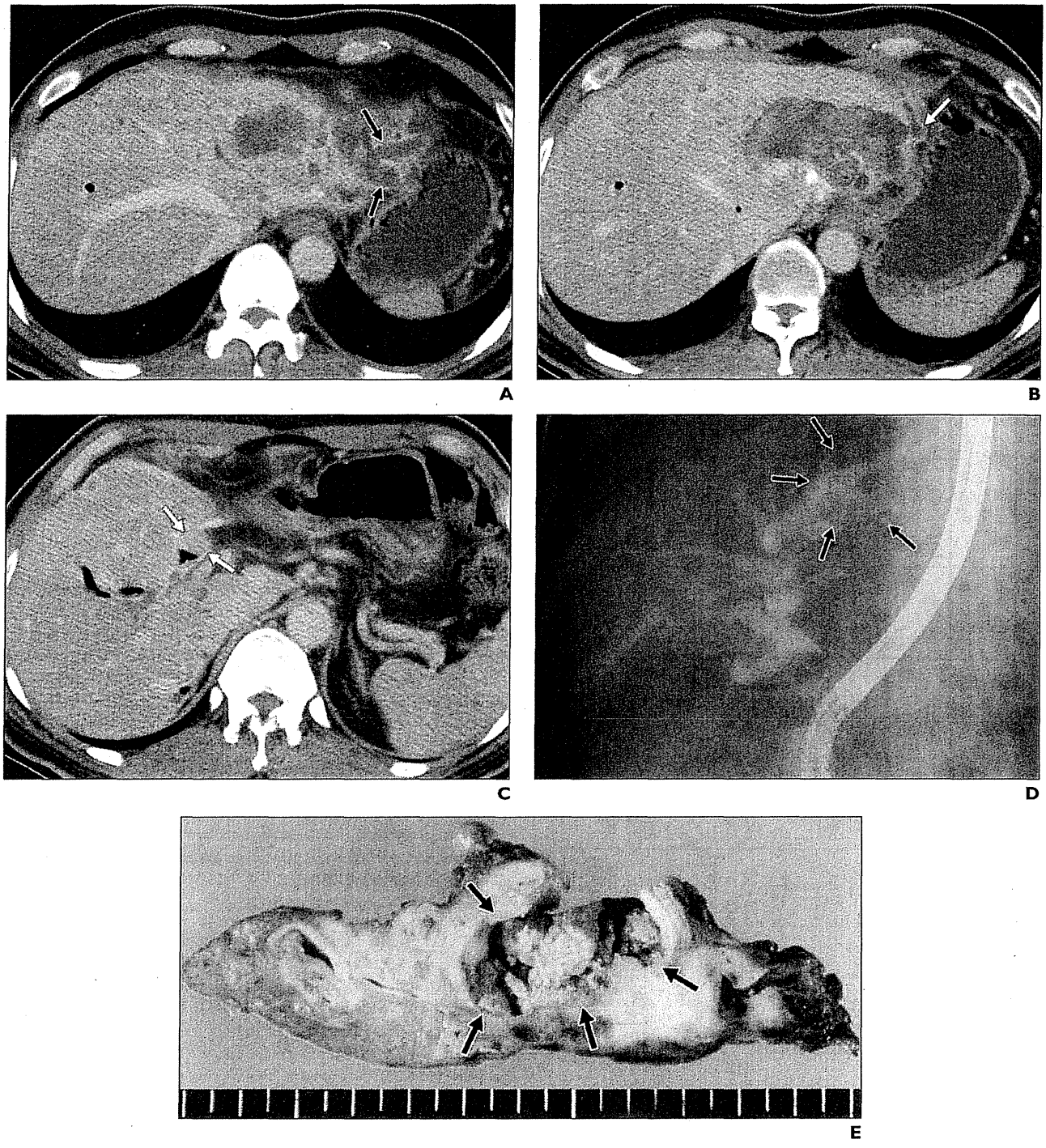

Fig. 1—53-year-old man with intraductal papillary neoplasm of the bile duct (carcinoma).
A and **B,** Contrast-enhanced CT images show oval cystic mass containing multiple papillary tumors and fluid inside lateral segment of left hepatic lobe. Note dilatation of bile ducts (*arrows,* **A** and **B**) peripheral to cystic tumor with direct communication.
C, CT image acquired 3 cm below that in panel **B** shows small tumor (*arrows*) in left hepatic duct occluding the duct. Air in left hepatic ducts distal to tumor is a result of previous ERCP.
D, ERCP image shows markedly dilated intra- and extrahepatic ducts. Note filling defect (*arrows*) within lateral segmental bile duct (B2), representing papillary tumor inside cystically dilated bile duct. Large filling defects in common bile duct are air bubbles.
E, Photograph of resected specimen shows cystic tumor and papillary tumors inside (*arrows*). Aneurysmally dilated cystic cavity was continuous with dilated proximal and distal bile ducts.

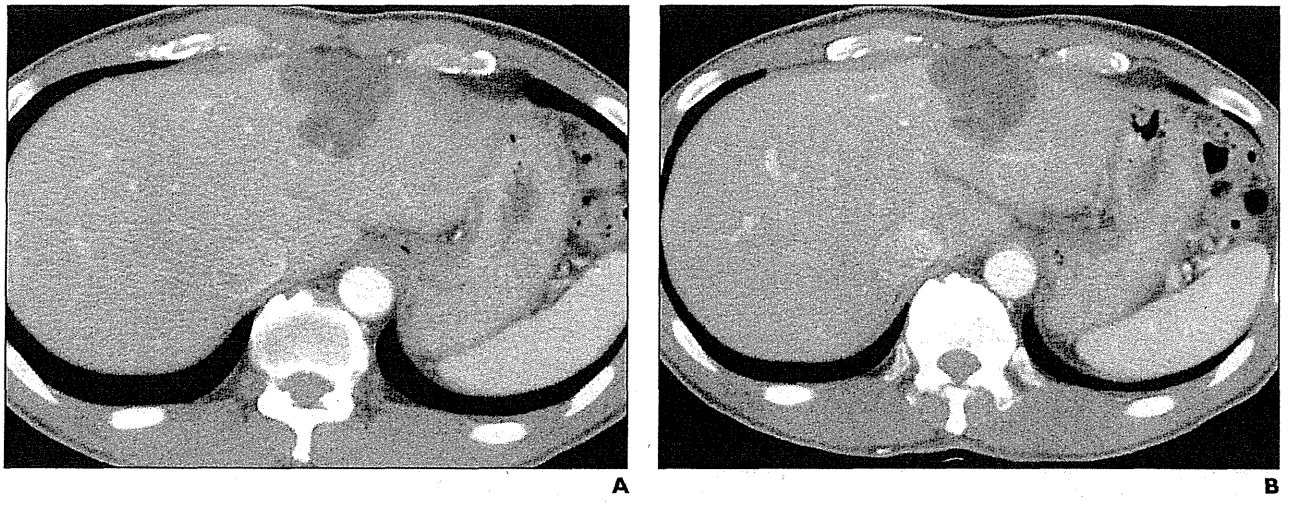

A B

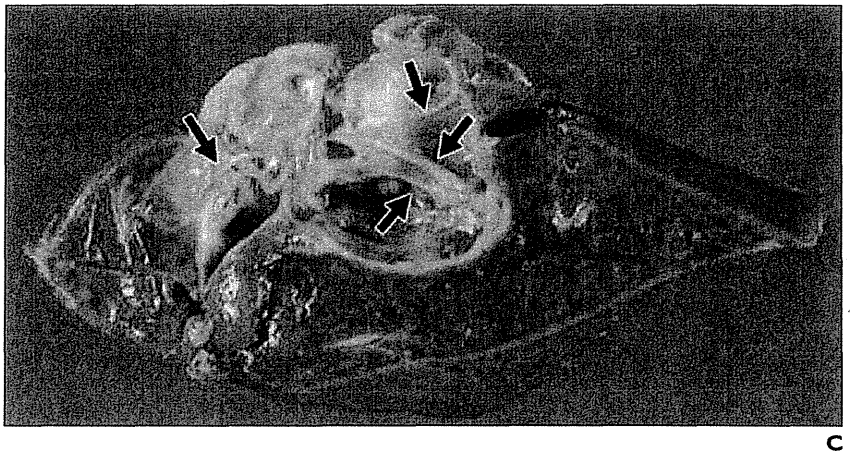

C

Fig. 2—46-year-old man with intraductal papillary neoplasm of the bile duct (carcinoma, confined to wall).
A and **B**, Contrast-enhanced transverse CT images show bile duct multiloculated cystic tumor containing thin septae and small excrescences. Bile ducts are not dilated.
C, Resected specimen shows multiloculated cyst containing thin septae and flat tumor with papillary surface (*arrows*).

and multislab thin-section images were obtained using a single-shot fast spin-echo sequence. Using coronal multislab fast spin-echo and single-shot fast spin-echo sequences, source images were processed on a console using maximum-intensity-projection reconstruction, including target-volume maximum-intensity projection. Vascular MRI contrast agent was administered in two patients, and hepatobiliary-specific contrast agent was administered in one patient.

ERCP—ERCP was performed on four patients by gastroenterologists using a duodenoscope (EVIS JF-200, Olympus). Ionic contrast material (60% iothalamate meglumine; Renografin-60, Bracco) was used after 50% dilution.

Image Interpretation

Two gastrointestinal radiologists with 24 and 10 years of experience in hepatobiliary imaging reviewed CT, ultrasound, ERCP, and MRCP images during one interpretation session. For 10 patients, images were reviewed on a 2000 × 2000-pixel PACS (Centricity, GE Healthcare Integrated Imaging Solutions), with adjustment of optimal window settings and a stack-view system. For two patients who underwent CT at outside hospitals, hard-copy films were used in interpretation.

The two radiologists were aware that the patients had biliary IPN before image interpretation, but they were unaware of the pathologic findings. Decisions regarding imaging features were determined in consensus. The two radiologists evaluated bile duct tumors in terms of the size of the cyst, relationship of the cystic tumors to the bile ducts, shape of intracystic tumors, bile duct dilatation, communication between a cystic lesion and bile duct, and the presence of mucin in the downstream bile duct on ERCP images.

Pathologic Evaluation

Surgical records, photographs of resected specimens, and pathology reports were available for all patients. A pathologist who subspecialized in the biliary system and pancreas for 11 years reviewed the macroscopic characteristics of biliary cystic tumors (unilocular or multilocular), cyst content, and intracystic tumors (fungating mass or excrescences). Special attention was paid to the relationship of cystic tumors to bile ducts and communication between the cystic tumor and the bile ducts.

Histopathologic characteristics were examined using routine H and E staining. Pathologic criteria of biliary intraductal papillary tumors were papillary proliferation of dysplastic epithelium along slender fibrovascular stalks, exhibiting innumerable papillary frondlike infoldings into the lumen of the bile duct, or cystic mass. The presence of ovarian-like stroma in the capsule of the cyst was investigated. Histopathologic phenotypes were classified into four types as pancreaticobiliary, intestinal, gastric, and oncocytic, according to the pathologic characteristics of intraductal papillary mucinous neoplasms of the pancreas [24].

Features Suggestive of the Peribiliary Gland Origin

If a cystic tumor arises from peribiliary glands, a diverticulum-like appearance would be expected.

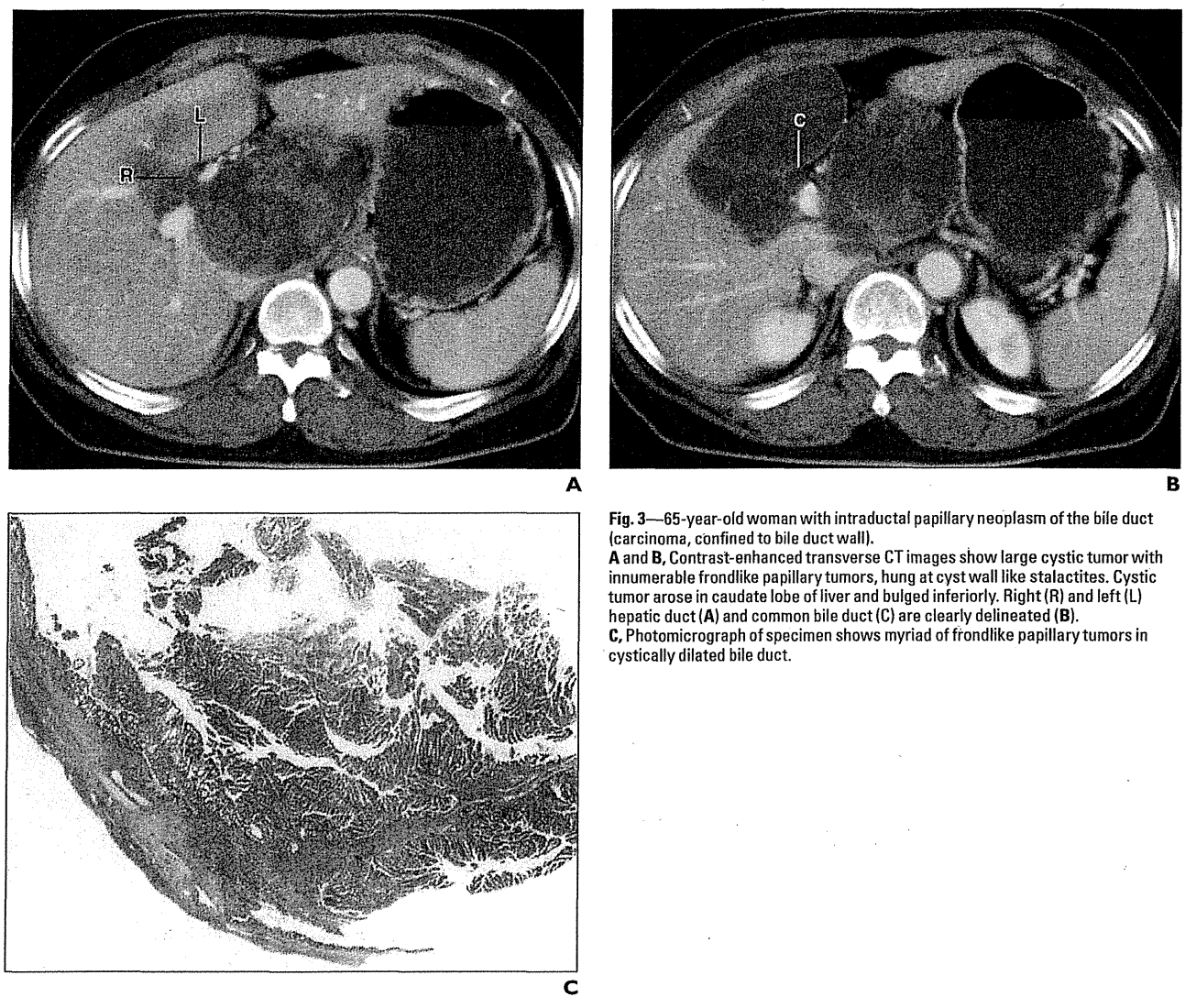

Fig. 3—65-year-old woman with intraductal papillary neoplasm of the bile duct (carcinoma, confined to bile duct wall).
A and **B**, Contrast-enhanced transverse CT images show large cystic tumor with innumerable frondlike papillary tumors, hung at cyst wall like stalactites. Cystic tumor arose in caudate lobe of liver and bulged inferiorly. Right (R) and left (L) hepatic duct (**A**) and common bile duct (C) are clearly delineated (**B**).
C, Photomicrograph of specimen shows myriad of frondlike papillary tumors in cystically dilated bile duct.

Thus, the presence or absence of such an appearance was examined radiologically and macroscopically in each case. Given the lack of a marker specifically expressed in peribiliary glands, it is difficult to histologically examine this possibility, particularly for the large cystic tumors examined in this study.

Results

Imaging Features

Cystic tumors involved the right and left hepatic ducts in two patients, the left hepatic duct only in another two patients, and the left hepatic and caudate lobar ducts in one patient. In six patients, cystic tumors involved segmental bile ducts: the right posterior segmental bile duct in one patient, the lateral segmental bile duct of the left lobe in four patients, and the caudate lobe bile duct in one patient. In one patient, a cystic tumor was attached to the extrahepatic duct. Cystic tumor size ranged from 4 to 17 cm in greatest diameter (mean, 8.3 cm). A multilocular cystic lesion (Figs. 1 and 2) was observed in five patients, and a unilocular cystic lesion (Figs. 3–5) was observed in seven patients. Each locule was distinct on CT and ultrasound images and was separated by thin septae (Figs. 1 and 2).

Regarding the relationship of cystic lesions to the bile ducts, tumor-bearing bile ducts showed cystic or balloonlike dilatation (Fig. 1) in five patients (patients 2, 3, 4, 7, and 12). The dilated cystic lesions were lobulated or multiloculated. In five patients (patients 1 and 8–11), dilated cystic lesions were attached to the bile duct like a diverticulum (Figs. 4 and 5); communication was observed between the cystic lesions and the bile ducts in two of those patients, but in three patients, there was no communication. In the remaining two patients (patients 5 and 6), the spatial relationship of the cystic lesions to the bile ducts was not clear because the cyst was large but the cyst-bearing bile ducts were not dilated but rather narrow (Figs. 2 and 3); thus, the relationship was obscure.

In six patients, CT, MRI, and ERCP scans showed communication between the cystic lesion and bile ducts, whereas in another six patients, there was no visible communication. In three patients, tumor masses were observed at the site of communication between the cyst and the bile duct (Fig. 4).

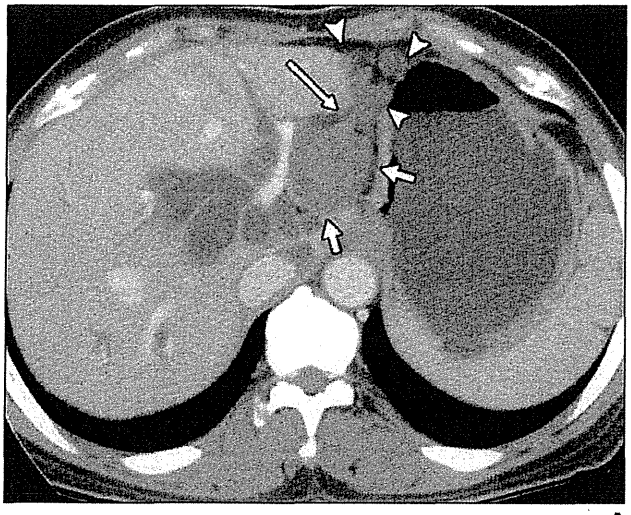

A

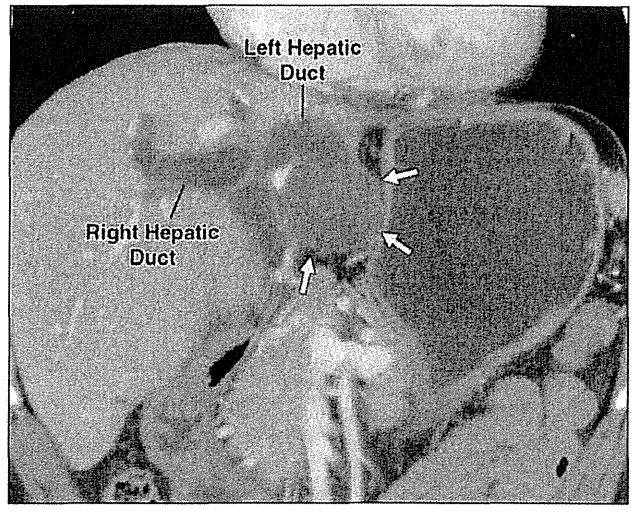

B

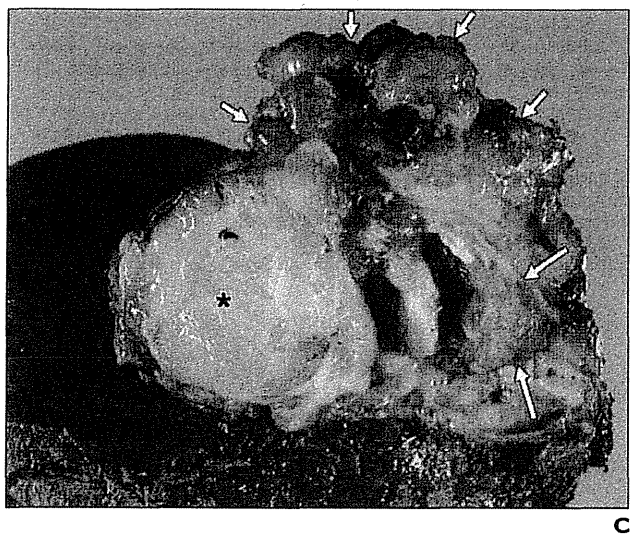

C

Fig. 4—49-year-old woman with intraductal papillary neoplasm of the bile duct (carcinoma, focally invasive).
A, Contrast-enhanced transverse CT image shows diverticulum-like cystic tumor attached to left hepatic duct (*short arrows*) containing faintly opacified soft-tissue tumor. Part of cyst or branch of bile duct ruptured (*long arrow*) and multilobulated collections of fluid (mucin) were observed at liver surface (*arrowheads*).
B, Contrast-enhanced coronal CT image shows eccentrically located diverticulum-like cystic tumor attached to dilated left hepatic duct, bulged out from liver (*arrows*). Note faintly visualized soft-tissue tumor contained within dilated bile duct.
C, Cut surface of resected specimen shows multilobulated mucin collections in liver surface (*short arrows*), mucin plug (*asterisk*), and papillary tumor (*long arrows*) in aneurysmally dilated left hepatic duct.

Within cystic lesions, fungating papillary masses (Figs. 1 and 5) were observed in five patients, and multiple shallow papillary excrescences (Figs. 2–4) were attached to the capsule in six patients. In one patient, there was no mass or excrescence in the cyst wall. Papillary masses or excrescences showed variable enhancement. In one patient in whom hepatobiliary-specific contrast agent was administered, the papillary masses were highly enhanced in the arterial dominant phase, but the mass did not take up contrast agent in the hepatobiliary phase. The remaining cystic spaces presented as clear fluid-containing spaces. For two patients with invasive carcinoma at histologic analysis, there was no difference in imaging findings from those of the patients with no invasion at histologic analysis.

Bile ducts showed moderate or marked dilatation in six patients; dilatation in only the upstream bile ducts was observed in one patient, and in both upstream and downstream bile ducts in five patients (Figs. 1 and 4). In six patients, there was no bile duct dilatation (Figs. 2, 3, and 5). In five patients, a large amount of mucin was observed in the downstream bile ducts on cholangiogram or duodenal endoscopy; on cholangiogram, mucin appeared as elongated or noodlelike filling defects.

Surgical and Gross Findings

During surgery, six cystic lesions were found in the left hepatic lobe, one in the right lobe, one in the caudate lobe, and one in the left and caudate lobe. Two cystic lesions were found in the dilated right and left hepatic ducts per se. In one patient (patient 11), the cystic lesion was attached to the common hepatic duct with an overall diverticulum-like appearance (Fig. 5). Depending on the location of cystic lesions, left hemihepatectomy, right hemihepatectomy, left hepatic and caudate lobectomy, caudate lobectomy, trisectionectomy, or resection of the extrahepatic duct were performed. In one patient, several lobulated mucin collections were noted at the liver surface in association with perihepatic adhesions (Fig. 4).

On gross examination of pathologic specimens, cystic lesions measured 8 cm in diameter on average (range, 4–17 cm). In five cases, cysts were multilocular or were multiloculated in appearance, and in seven cases,

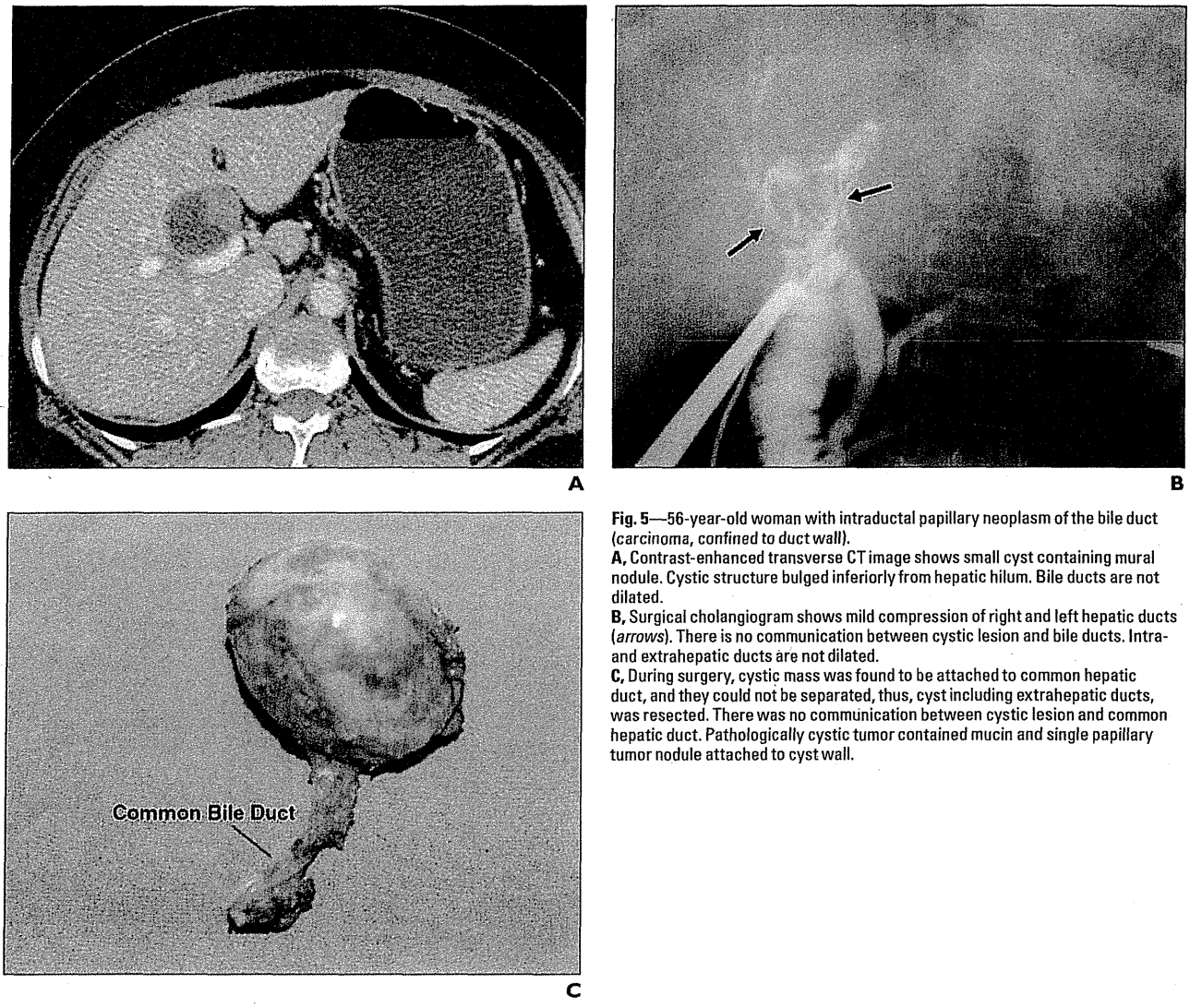

Fig. 5—56-year-old woman with intraductal papillary neoplasm of the bile duct (*carcinoma, confined to duct wall*).
A, Contrast-enhanced transverse CT image shows small cyst containing mural nodule. Cystic structure bulged inferiorly from hepatic hilum. Bile ducts are not dilated.
B, Surgical cholangiogram shows mild compression of right and left hepatic ducts (*arrows*). There is no communication between cystic lesion and bile ducts. Intra- and extrahepatic ducts are not dilated.
C, During surgery, cystic mass was found to be attached to common hepatic duct, and they could not be separated, thus, cyst including extrahepatic ducts, was resected. There was no communication between cystic lesion and common hepatic duct. Pathologically cystic tumor contained mucin and single papillary tumor nodule attached to cyst wall.

cystic lesions were unilocular. Communication between cystic spaces and the bile duct was present in five cases, as seen on images; however, in the other seven cases, communication could not be grossly confirmed. In two cases, multilocular cystic lesions were the cystically or aneurysmally dilated right and left hepatic ducts per se, and the dilated ducts were lined by innumerable papillary tumors and excrescences (Fig. 1). In the other four cases showing communication with bile ducts, lobulated cystic lesions abutted the tumor-bearing bile duct eccentrically (Fig. 4). All cystic lesions contained mucinous or mucopurulent fluid. Internal septae were observed in three cases of multilocular cystic lesions (Fig. 2). In one case, bile ducts were ruptured and a multiloculated collection of mucin, not a cystic tumor, was present at the surface of the liver (Fig. 4). In the interior of cystic lesions, single nodular or multiple fungating masses or excrescences, ranging from 0.5 to 2 cm, showing granular surfaces were observed (Figs. 1–4). In one patient, there was no mural nodule or excrescence in the cystic lesion.

Features Suggestive of the Peribiliary Gland Origin

A diverticulum-like appearance was radiologically identified in five patients (42%) (patients 1 and 8–11) and was also macroscopically confirmed in one patient (patient 11) (Fig. 5). It was impossible to macroscopically identify that appearance in the other four patients, in whom cystic tumors were predominantly located in the liver.

Histologic Findings

On histologic examination, prominent papillary proliferation with delicate fibrovascular core was observed in mural nodules or papillary excrescences along the cyst walls (Fig. 3). In one patient, there was no gross tumor; however, on microscopic examination, the internal surface showed flat papillary epithelial proliferation with fibrovascular cores. None of the cases showed ovarian stroma in the cyst wall.

Tumor cells consisted of columnar epithelium showing increased nuclear-to-cytoplasmic ratios, irregularity of the nuclear membrane,

and occasional mitotic figures. Intracytoplasmic mucin was also noted in places. Ten cases were morphologically papillary carcinoma in situ, whereas the remaining two cases (patients 8 and 12) were associated with invasive foci of mucinous carcinoma (Fig. 4). Regarding phenotypes, four cases were pancreaticobiliary, as evidenced by eosinophilic cytoplasm and round nuclei. Three oncocytic cases showed oxyphilic cytoplasm and round nuclei located in the center of tumor cells. The remaining four cases consisted of neoplastic columnar epithelium with nuclear stratification and occasional goblet cells, with the overall appearance resembling intestinal adenocarcinoma. No gastric type of tumor was identified in this study.

A summary of the clinical, radiologic, surgical, and pathologic findings is presented in Table 1.

Discussion

IPN of the bile duct exhibits intraluminal tumor growth, often spreading superficially along the mucosal surface, and results in polypoid or sessile growth, sometimes filling the lumen like a cast [10]. In cystic variants of IPN of the bile duct, the tumor forms a large mucin-containing cyst, and the inner surface of the cyst is lined by tumor cells showing papillary configurations. There have been several reports of cyst-forming mucin-hypersecreting IPNs of the bile duct in the liver [9, 11–14, 23, 25] resembling intraductal papillary mucinous neoplasms of the pancreas. It has been speculated that IPN of the bile duct and pancreatic intraductal papillary mucinous neoplasm share common morphologic findings, histopathologic features, biologic characteristics, and clinical manifestations [13, 26]. Indeed, the literature has addressed intraductal papillary mucinous tumors simultaneously involving the bile ducts as well as the pancreatic duct [27, 28].

There have been several articles describing a good prognosis for patients with IPN of the bile duct after surgical resection [5, 6, 25]. This is probably because, in IPN of the bile duct, tumors do not penetrate and invade the bile duct wall until the IPNs of the bile duct transform to invasive tubular adenocarcinoma or mucinous adenocarcinoma. However, to our knowledge, there has been no study of the clinical features and postoperative prognosis of cyst-forming IPN of the bile duct involving a considerable number of patients.

In the present study, we observed gross morphologic, histopathologic, and biologic similarities between IPN of the bile duct and intraductal papillary mucinous neoplasm of the pancreas and confirmed previous reports that IPN of the bile duct could be a counterpart to intraductal papillary mucinous neoplasm of the pancreas [18, 29]. Similar findings in both diseases included intraductal papillary epithelial proliferation with fibrovascular core, lack of ovarian stroma in the cyst wall, the same histologic phenotypes, mucin overproduction, and a tendency toward progression to invasive adenocarcinoma. Zen et al. [26, 29] reported pathologic similarities and differences and concluded that a cystic variant of IPN of the bile duct associated with bile duct communication might be a counterpart to intraductal papillary mucinous neoplasm of the pancreas. Of interest is that five patients showed a diverticulum-like appearance, which is suggestive of the peribiliary gland origin. As described previously in this article, given the potential biologic similarity between peribiliary glands and pancreatic branch ducts, it is fair to say that at least some of the cyst-forming IPNs of the bile duct belong to the biliary counterpart of the branch type of intraductal papillary mucinous neoplasms of the pancreas. However, surgical resection is necessary for cyst-forming IPNs of the bile duct, in contrast to the branch of type intraductal papillary mucinous neoplasm of the pancreas, because most cases of IPN of the bile duct are at least carcinoma in situ.

Why, then, does IPN of the bile duct exhibit cystic tumor formation rather than localized segmental dilatation of affected bile ducts? Whatever the origin of tumors in the biliary tract, cystic or aneurysmal dilatation is a result of increased intraductal pressure, which is caused by excessive mucin production by a papillary tumor. When a mucin-producing IPN of the bile duct arises in a relatively large bile duct, the affected bile ducts become dilated as a result of tumor bulk [23] and stagnated viscid mucin [9]. Mucin is mostly thick and viscid, and drainage through the downstream bile ducts is hampered; thus, the tumor-harboring bile ducts may be disproportionately more dilated and become cystic or aneurysm-like (Fig. 1). In these cases, lobar or segmental bile ducts become a part of the cystic tumor (patients 2, 3, 4, 7, and 12 in our series). The degree of dilatation depends on the amount of mucin production and intraductal pressure.

As an alternative morphogenesis of cyst-forming IPN of the bile duct, some of this type of IPN may arise from the peribiliary glands located within the wall of or scattered in the surrounding connective tissue of the intrahepatic large bile duct and extrahepatic bile ducts [30–32]. They are branched tubuloalveolar seromucous glands [32]. These glands are shown to connect to the adjacent large bile duct by their own conduits. When papillary and mucin-secreting tumors arise in the peribiliary glands of the large intrahepatic and extrahepatic bile ducts, the tumor in the peribiliary glands may thus partially or completely occlude their conduits by their compression and possible twisting; thus, their connection to the lumen of the large bile duct will be easily blocked. Because of continuous mucin production and secretion, peribiliary glands and their conduits showed progressive dilation, which is filled with mucin, resembling a diverticulum as seen in five patients in this study. In fact, Nakanuma [18] and Nakanuma et al. [33] have already reported that multiple cystic lesions arise from these peribiliary glands and that some of these cysts show apparently neoplastic proliferation of glandular cells. As additional supporting evidence, Zen et al. [26, 29] reported an interesting observation that some cases of cyst-forming IPN of the bile duct were associated with glandular tissues resembling peribiliary glands in the cyst wall. Recently, Nakanishi et al. [34] reported a case of oncocytic IPN of the bile duct arisen from a cystically dilated peribiliary gland.

This postulation may explain the morphogenesis of diverticulum-like IPN of the bile ducts in our series (patients 1 and 8–11), explaining that mucinous tumor might have arisen from the peribiliary glands: connection to the bile duct was patent in three patients (patients 1, 8, and 9), but in two patients (patients 10 and 11), connection might have been disrupted, as speculated previously in this article. In particular, one patient (patient 11) (Fig. 5) had a cystic mucinous tumor attached to the extrahepatic duct, but the connection was obliterated. In the remaining two patients (patients 5 and 6), the relationship of the cystic lesion to the tumor-bearing bile ducts was not clear; however, it is possible that the cystic IPN of the bile duct might have arisen from the peribiliary glands and that the connection was blocked.

There are some inherent limitations in this study. First, a retrospective study cannot control the handling of pathologic specimens as in a prospective and objective-oriented study. Sometimes, tumor fragments or mucin may be detached from the specimen. Although

photographs of all pathologic specimens were available, there were still limitations in the evaluation of detailed anatomic and pathologic status and in using standard imaging methods. Second, communication between cystic lesions and bile ducts was evaluated by imaging such as CT, MRI, and ERCP. Communication with a wide opening was obvious on imaging, but communication with a narrow opening might have not been seen. Such a narrow communication cannot be confirmed macroscopically because demonstration of the ductal communication is almost impossible with gross examination or probing [26]. Third, independent blind review of images by radiologists could have been considered to allow evaluation of interobserver variability, but we did not assess the interobserver variability because of the small cohort.

In conclusion, we evaluated the morphologic appearances of IPNs of the bile duct by imaging and evaluation of gross pathologic specimens and performed histopathologic examination with regard to their similarity to cyst-forming pancreatic branch-duct intraductal papillary mucinous neoplasm. This study suggests that at least some cyst-forming IPNs of the bile duct might arise from peribiliary glands and be a counterpart of the branch type of intraductal papillary mucinous neoplasm of the pancreas, given the diverticulum-like appearance.

References

1. Korobkin M, Stephens DH, Lee JK, et al. Biliary cystadenoma and cystadenocarcinoma: CT and sonographic findings. *AJR* 1989; 153:507–511
2. Buetow PC, Buck JL, Pantongrag-Brown L, et al. Biliary cystadenoma and cystadenocarcinoma: clinical-imaging-pathologic correlations with emphasis on the importance of ovarian stroma. *Radiology* 1995; 196:805–810
3. Mortele KJ, Ros PR. Cystic focal liver lesions in the adult: differential CT and MR imaging features. *RadioGraphics* 2001; 21:895–910
4. Bosman FT, Carneiro F, Hurban RH, Theise ND, eds. *WHO classification of tumours of digestive system.* Lyon, France: International Agency for Research on Cancer Press, 2010: 222–224, 236–238
5. Nakanuma Y, Sasaki M, Ishikawa A, Tsui W, Chen TC, Huang SF. Biliary papillary neoplasm of the liver. *Histol Histopathol* 2002; 17:851–861
6. Chen TC, Nakanuma Y, Zen Y, et al. Intraductal papillary neoplasia of the liver associated with hepatolithiasis. *Hepatology* 2001; 34:651–658
7. Zen Y, Sasaki M, Fujii T, et al. Different expression patterns of mucin core proteins and cytokeratins during intrahepatic cholangiocarcinogenesis from biliary intraepithelial neoplasia and intraductal papillary neoplasm of the bile duct—an immunohistochemical study of 110 cases of hepatolithiasis. *J Hepatol* 2006; 44:350–358
8. Shimonishi T, Zen Y, Chen TC, et al. Increasing expression of gastrointestinal phenotypes and p53 along with histologic progression of intraductal papillary neoplasia of the liver. *Hum Pathol* 2002; 33:503–511
9. Lim JH, Yoon KH, Kim SH, et al. Intraductal papillary mucinous tumor of the bile ducts. *RadioGraphics* 2004;24:53–66, discussion 66–67
10. Lim JH, Jang KT. Mucin-producing bile duct tumors: radiological-pathological correlation and diagnostic strategy. *J Hepatobiliary Pancreat Sci* 2010; 17:223–229
11. Terada T, Taniguchi M. Intraductal oncocytic papillary neoplasm of the liver. *Pathol Int* 2004; 54:116–123
12. Aoki S, Okayama Y, Kitajima Y, et al. Intrahepatic biliary papilloma morphologically similar to biliary cystadenoma. *J Gastroenterol Hepatol* 2005; 20:321–324
13. Yamashita Y, Fukuzawa K, Taketomi A, et al. Mucin-hypersecreting bile duct neoplasm characterized by clinicopathological resemblance to intraductal papillary mucinous neoplasm (IPMN) of the pancreas. *World J Surg Oncol* 2007; 5:98
14. Kim HJ, Kim MH, Lee SK, et al. Mucin-hypersecreting bile duct tumor characterized by a striking homology with an intraductal papillary mucinous tumor (IPMT) of the pancreas. *Endoscopy* 2000; 32:389–393
15. Augustin T, Vandermeer TJ. Intraductal papillary mucinous neoplasm: a clinicopathologic review. *Surg Clin North Am* 2010; 90:377–398
16. Basturk O, Coban I, Adsay NV. Pancreatic cysts: pathologic classification, differential diagnosis, and clinical implications. *Arch Pathol Lab Med* 2009; 133:423–438
17. Procacci C, Carbognin G, Biasiutti C, Guarise A, Ghirardi C, Schenal G. Intraductal papillary mucinous tumors of the pancreas: spectrum of CT and MR findings with pathologic correlation. *Eur Radiol* 2001; 11:1939–1951
18. Nakanuma Y. A novel approach to biliary tract pathology based on similarities to pancreatic counterparts: is the biliary tract an incomplete pancreas? *Pathol Int* 2010; 60:419–429
19. Oshikiri T, Kashimura N, Katanuma A, et al. Mucin-secreting bile duct adenoma: clinicopathological resemblance to intraductal papillary mucinous tumor of the pancreas. *Dig Surg* 2002; 19: 324–327
20. Shibahara H, Tamada S, Goto M, et al. Pathologic features of mucin-producing bile duct tumors: two histopathologic categories as counterparts of pancreatic intraductal papillary-mucinous neoplasms. *Am J Surg Pathol* 2004; 28:327–338
21. Kloppel G, Kosmahl M. Is the intraductal papillary mucinous neoplasia of the biliary tract a counterpart of pancreatic papillary mucinous neoplasm? *J Hepatol* 2006; 44:249–250
22. Lim JH, Kim YI, Park CK. Intraductal mucosal-spreading mucin-producing peripheral cholangiocarcinoma of the liver. *Abdom Imaging* 2000; 25:89–92
23. Lim JH, Jang KT, Rhim H, Kim YS, Lee KT, Choi SH. Biliary cystic intraductal papillary mucinous tumor and cystadenoma/cystadenocarcinoma: differentiation by CT. *Abdom Imaging* 2007; 32:644–651
24. Furukawa T, Kloppel G, Volkan Adsay N, et al. Classification of types of intraductal papillary-mucinous neoplasm of the pancreas: a consensus study. *Virchows Arch* 2005; 447:794–799
25. Lee SS, Kim MH, Lee SK, et al. Clinicopathologic review of 58 patients with biliary papillomatosis. *Cancer* 2004; 100:783–793
26. Zen Y, Fujii T, Itatsu K, et al. Biliary cystic tumors with bile duct communication: a cystic variant of intraductal papillary neoplasm of the bile duct. *Mod Pathol* 2006; 19:1243–1254
27. Hubens G, Delvaux G, Willems G, Bourgain C, Kloppel G. Papillomatosis of the intra- and extrahepatic bile ducts with involvement of the pancreatic duct. *Hepatogastroenterology* 1991; 38:413–418
28. Joo YH, Kim MH, Lee SK, et al. A case of mucin-hypersecreting intrahepatic bile duct tumor associated with pancreatic intraductal papillary mucinous tumor. *Gastrointest Endosc* 2000; 52: 409–412
29. Zen Y, Fujii T, Itatsu K, et al. Biliary papillary tumors share pathological features with intraductal papillary mucinous neoplasm of the pancreas. *Hepatology* 2006; 44:1333–1343
30. Nakanuma Y, Hoso M, Sanzen T, Sasaki M. Microstructure and development of the normal and pathologic biliary tract in humans, including blood supply. *Microsc Res Tech* 1997; 38:552–570
31. Healey JE Jr, Schroy PC. Anatomy of the biliary ducts within the human liver; analysis of the prevailing pattern of branchings and the major variations of the biliary ducts. *AMA Arch Surg* 1953; 66:599–616
32. Terada T, Nakanuma Y, Ohta G. Glandular elements around the intrahepatic bile ducts in man; their morphology and distribution in normal livers. *Liver* 1987; 7:1–8
33. Nakanuma Y, Kurumaya H, Ohta G. Multiple cysts in the hepatic hilum and their pathogenesis: a suggestion of periductal gland origin. *Virchows Arch A Pathol Anat Histopathol* 1984; 404:341–350
34. Nakanishi Y, Zen Y, Hirano S, et al. Intraductal oncocytic papillary neoplasm of the bile duct: the first case of peribiliary gland origin. *J Hepatobiliary Pancreat Surg* 2009; 16:869–873

The American Journal of Pathology, Vol. 179, No. 6, December 2011

DOI: 10.1016/j.ajpath.2011.08.028

Gastrointestinal, Hepatobiliary, and Pancreatic Pathology

Biliary Infection May Exacerbate Biliary Cystogenesis Through the Induction of VEGF in Cholangiocytes of the Polycystic Kidney (PCK) Rat

Xiang Shan Ren,*† Yasunori Sato,* Kenichi Harada,* Motoko Sasaki,* Norihide Yoneda,*‡ Zhen Hua Lin,† and Yasuni Nakanuma*

From the Departments of Human Pathology and Radiology,‡ Kanazawa University Graduate School of Medicine, Kanazawa, Japan; and the Department of Pathology,† Yanbian University College of Medicine, Yanji-City, China*

Cholangitis arising from biliary infection dominates the prognosis in Caroli's disease. To clarify the influences of bacterial infection on the biliary cystogenesis, *in vivo* and *in vitro* studies were performed using the polycystic kidney (PCK) rat as an animal model of Caroli's disease. Cholangitis became a frequent histological finding in aged PCK rats, and neovascularization around the bile ducts also increased in aged PCK rats. Immunohistochemistry revealed that expression of vascular endothelial growth factor (VEGF) was increased in PCK rat biliary epithelium. *In vitro*, PCK cholangiocytes overexpressed VEGF, and the supernatant of cultured PCK cholangiocytes significantly increased the proliferative activity, migration, and tube formation of cultured rat vascular endothelial cells. Stimulation with lipopolysaccharide (LPS) further induced VEGF expression in PCK cholangiocytes, which might be mediated by signaling pathways involving phosphatidylinositol 3-kinase (PI3K)-Akt and c-Jun N-terminal kinase (JNK). Both LPS and VEGF increased cell proliferative activity in PCK cholangiocytes, and siRNA against VEGF significantly reduced LPS-induced cell proliferation. Thus, LPS-induced overexpression of VEGF in the biliary epithelium may lead to hypervascularity around the bile ducts; concurrently, LPS and VEGF act as cell proliferation factors for cholangiocytes. Biliary infection may thus exacerbate biliary cystogenesis in PCK rats. *(Am J Pathol 2011, 179:2845–2854; DOI: 10.1016/j.ajpath.2011.08.028)*

Caroli's disease is characterized by progressive, multiple cystic dilation of intrahepatic bile ducts; it is frequently associated with portal fibrosis, corresponding to congenital hepatic fibrosis.[1,2] Caroli's disease belongs to a group of congenital hepatorenal fibrocystic syndromes, and is a well-known hepatic manifestation of autosomal recessive polycystic kidney disease (PKD).[3]

Caroli's disease with congenital hepatic fibrosis presents clinical features consisting of bouts of cholangitis and cholelithiasis and portal hypertension. Clinical progression and presentation are highly variable, and symptoms may appear early or late in life. Bile stagnation due to bile duct dilation and hepatolithiasis explains the recurrent cholangitis that dominates the clinical course and is the principal cause of morbidity and mortality. Cholangitis can lead to hepatic abscess and sepsis, and a large number of patients die within 5 to 10 years after cholangitis occurs in Caroli's disease.[4]

Human and experimental data suggest several potential mechanisms that could lead to cystic dilation of intrahepatic bile ducts of Caroli's disease. These include increased cell proliferation and apoptosis, enhanced fluid secretion, abnormal cell-matrix interactions, and abnormal ciliary structure or function.[5–9] Although the clinical significance of cholangitis due to biliary infection is well recognized in Caroli's disease, the effect of biliary infection on disease pathogenesis and progression has not been studied previously.

Lipopolysaccharide (LPS) is a bacterial component that is a proximal mediator in the initiation of local inflammation and sepsis. LPS induces production of proinflammatory cytokines and permeability factors. In certain types of cells, LPS induces angiogenic factors, such as vascular endothelial growth factor (VEGF).[10,11] Because cholangiocytes express the receptor of LPS, Toll-like receptor 4 (TLR4),[12,13] LPS may also be able to induce angiogenic growth factors in cholangiocytes.

VEGF is overexpressed in human and rodent cholangiocytes from polycystic liver diseases, including Caroli's

Accepted for publication August 4, 2011.

Address reprint requests to Yasuni Nakanuma, M.D., Ph.D., Department of Human Pathology, Kanazawa University Graduate School of Medicine, 13-1 Takara-machi, Kanazawa 920-8640, Japan. E-mail: pbcpsc@kenroku.kanazawa-u.ac.jp.

disease, and has been implicated in disease pathogenesis.[14] Overexpression of VEGF in cholangiocytes indicates that VEGF may induce portal neovascularization, which leads to cholangiocyte overgrowth due to abundant vascular supply, in turn resulting in the exacerbation of cystic bile duct dilation. In addition, a recent study showed that VEGF stimulates cholangiocyte proliferation via an autocrine mechanism.[15]

Using the polycystic kidney (PCK) rat as an animal model of Caroli's disease,[5] we conducted the present study to clarify the influences of bacterial infection on the biliary cystogenesis with regard to VEGF expression in cholangiocytes and portal neovascularization.

Materials and Methods

Animals

The PCK rats were maintained at the laboratory animal institute of Kanazawa University Graduate School of Medicine. Normal (Crj:CD) rats were purchased from Charles River Japan (Sagamihara, Japan). Animal studies were performed in accordance with guidelines for the care and use of laboratory animals at the Takara-machi Campus of Kanazawa University.

Liver Specimens

Livers were removed from 3-week-old, 2-month-old, and 10-month-old rats. Human liver tissues of Caroli's disease with congenital hepatic fibrosis (5 cases) were obtained at time of surgery. As controls, normal or subnormal human livers were used (n = 5). Liver tissues were immersed in 10% formalin neutral buffer solution (pH 7.4) and then embedded in paraffin. More than 10 serial sections (4 μm thick) cut from each paraffin block were subjected to histological analysis. Experiments using human subjects were performed with the approval of the local ethics committee of Kanazawa University under patient informed consent.

Cell Culture of Cholangiocytes

Cholangiocytes were isolated, purified, and cultured from the intrahepatic large bile ducts of normal and PCK rats as described previously.[6] Cells were set on cell culture dishes covered with a standard growth medium, composed of Dulbecco's modified Eagle's medium/F-12 (Gibco, Grand Island, NY) containing 10% bovine growth serum (HyClone, Logan, UT), 5 μmol/L forskolin (Wako Pure Chemical Industries, Osaka, Japan), 20 ng/mL of epidermal growth factor (Upstate Biotechnology; Millipore, Billerica, MA) and 1% antibiotic-antimycotic (Gibco) at 37°C in an atmosphere of 5% CO_2.

At subconfluent state, cholangiocytes were incubated with standard medium containing LPS (Ultra-Pure *E. coli* LPS; InvivoGen, San Diego, CA). Cell signaling inhibition studies were performed using NF-κB inhibitor (isohelenin; 30 μmol/L; Calbiochem, La Jolla, CA), VEGF receptor tyrosine kinase inhibitor (SU5614; 10 μmol/L; Sigma-Aldrich, St. Louis, MO), phosphatidylinositol 3-kinase (PI3K) inhibitor (LY294002; 20 μmol/L; Merck, Darmstadt, Germany), c-Jun N-terminal kinase (JNK) inhibitor I (2 μmol/L; Merck), and JNK inhibitor II (100 nmol/L; Merck).

Cell Culture of Vascular Endothelial Cells

Rat aorta endothelial cells (RAOECs) purchased from Cell Applications (San Diego, CA) were maintained with endothelial growth medium (rat endothelial cell basal medium; Cell Applications).

To determine their angiogenic effects, cholangiocytes were incubated with a standard medium for 3 days, and the culture supernatant was added to the basal medium of RAOECs at a concentration of 20%.

Cell Proliferation Assay

Cell proliferative activity was determined using a WST-1 assay according to the manufacturer's instructions (Roche, Mannheim, Germany). Cholangiocytes were treated with appropriate concentrations of LPS (InvivoGen) and recombinant VEGF (R&D Systems, Minneapolis, MN), and cell proliferative activity was determined at specified time intervals. Cell proliferative activity of RAOECs was assessed after 72 hours after stimulation with the cholangiocyte culture supernatant. WST-1 reagent was added and incubated for 2 hours before the plate was read. Each assay was performed in eight sets.

Cell Migration Assay

Cell migration activity of RAOECs was examined using a BioCoat cell migration chamber (BD Biosciences, Bedford, MA). In the upper chamber, a total of 5×10^4 cells in serum-free culture medium were seeded. In the lower chamber, rat endothelial cell basal medium (Cell Applications) or the basal medium containing 20% rat cholangiocyte culture supernatant with and without 24 hour-LPS treatment at the concentration of 1 μg/mL was placed. After 48 hours, cells were fixed in 100% methanol and were stained with hematoxylin. Cells that had migrated to the bottom side of the membrane were visualized under a light microscope, and the number of cells was counted in five randomly selected fields.

Tube Formation Assay

Tube formation assay was performed with use of growth-factor-reduced Matrigel (BD Biosciences). Matrigel was dispensed into a 24-well plate, and a total of 5×10^4 cells of RAOECs were placed on the gel. The cells were incubated with serum-free basal medium for 24 hours. The medium was changed then changed to the basal medium or to basal medium containing 20% rat cholangiocyte culture supernatant with and without 24 hour-LPS treatment at the concentration of 1 μg/mL; cells were then further incubated for 18 hours. The number of branching points of the cells was counted in five randomly selected fields.

Table 1. Primer Sequences and PCR Conditions

Gene	Sequences, forward and reverse	Annealing temperature (°C)	PCR cycles	Product size (bp)
VEGF	5′-AGTGGTCCCAGGCTGCAC-3′ 5′-TCCATGAACTTCCCACTTCGT-3′	60	40	70
Flk-1	5′-AAGGACCTCAGACGCAAGAA-3′ 5′-CATCCCAACACACAAAGCAC-3′	55	40	237
Flt-1	5′-AATCATTCCGAAGCAAGGTG-3′ 5′-TTTCTTCCCACAGTCCCAAC-3′	55	40	360
TLR4	5′-GCCGGAAAGTTATTGTGGTG-3′ 5′-TCCCACTCGAGGTAGGTGTT-3′	60	30	205
GAPDH	5′-GAGTCAACGGATTTGGTCGT-3′ 5′-TTGATTTTGGAGGGATCTC-3′	60	40	240

GAPDH, glyceraldehyde-3-phosphate dehydrogenase; TLR, Toll-like receptor; VEGF, vascular endothelial growth factor.

RT-PCR and Real-Time Quantitative PCR

RT-PCR was performed using total RNA (1 μg) extracted from the cholangiocytes. Total RNA was used to synthesize cDNA with reverse transcriptase (ReverTra Ace; Toyobo, Osaka, Japan). Primer sequences and PCR conditions are given in Table 1. The PCR products were subjected to 2% agarose gel electrophoresis and were stained with ethidium bromide.

Quantitative real-time PCR was performed according to a standard protocol using SYBR Green PCR master mix (Toyobo Co.) and an ABI Prism 7700 sequence detection system (PerkinElmer-Applied Biosystems, Warrington, UK). Cycling conditions were incubation at 50°C for 2 minutes, 95°C for 10 minutes, and 40 cycles of 95°C for 15 seconds and 60°C for 1 minute. Fold difference relative to GAPDH was calculated. Each assay was performed in five sets.

Western Blotting

Total proteins were extracted from cholangiocytes using Pierce T-PER protein extraction reagent (Thermo Fisher Scientific, Rockford, IL). The protein (40 μg) was subjected to 10% SDS-PAGE and then was electrophoretically transferred onto a nitrocellulose membrane. The membrane was incubated with primary antibodies against Akt, phosphorylated Akt (p-Akt), JNK-stress-activated protein kinase (SAPK), p-JNK-SAPK, extracellular signal-regulated kinase 1/2 (ERK1/2), p-ERK1/2, p38 mitogen-activated protein kinase (MAPK), and p-p38 MAPK. All primary antibodies (rabbit monoclonal) were purchased from Cell Signaling Technology (Danvers, MA) and were used at 1:1000 dilution. Protein expression was detected using a peroxidase-labeled polymer (EnVision+; DakoCytomation, Glostrup, Denmark), and 3,3′-diaminobenzidine tetrahydrochloride (DAB) was used as the chromogen.

ELISA

The VEGF level in the culture supernatant of the cholangiocytes was determined using an enzyme-linked immunosorbent assay (ELISA) kit (Quantikine rat VEGF immunoassay; R&D Systems). Samples were added to a 96-well plate coated with an antibody for VEGF and were incubated for 2 hours. After a washing, the plate was incubated with an anti-VEGF antibody conjugated to horseradish peroxidase for 2 hours. Color development was performed using a substrate solution for 30 minutes, and absorbance at 450 nm was measured. Each assay was performed in five sets.

Immunofluorescence Confocal Microscopy

Cells were fixed with 4% paraformaldehyde for 15 minutes and permeabilized for 3 minutes with 0.1% Triton X-100 surfactant. After blocking, the cells were incubated for 1 hour at room temperature with a primary antibody against VEGF (1:100, mouse monoclonal; Abcam, Cambridge, MA), NF-κB p50 (5 μg/mL, rabbit polyclonal; Immuno-Biological Laboratories, Fujioka, Japan), and NF-κB p65 (5 μg/mL, rabbit polyclonal; Immuno-Biological Laboratories). Alexa Fluor 488 (10 μg/mL, Invitrogen-Molecular Probes, Eugene, OR) was used as a secondary antibody. Nuclei were stained with DAPI.

NF-κB Activation

The activation of NF-κB was measured by the DNA binding capacity of NF-κB using a TransAM NF-κB kit according to the manufacturer's instructions (Active Motif, Carlsbad, CA). Briefly, cholangiocytes were treated with LPS (10 μg/mL) for 30 minutes, and the cell extract was added to an oligonucleotide-coated 96-well plate and incubated for 1 hour. After a washing, the NF-κB antibodies were added and incubated for 1 hour. The plate was then incubated with horseradish peroxidase-conjugated secondary antibody for 1 hour. Color development was performed using a developing solution for 30 minutes, and absorbance at 450 nm was measured. Each assay was performed in three sets.

VEGF Inhibition Studies

Synthetic VEGF siRNA and nonsilencing (negative control) siRNA were purchased from Qiagen (Tokyo, Japan). Transfections of siRNA were performed using HiPerFect transfection reagent (Qiagen) according to the manufacturer's instructions. Briefly, a total of 2×10^4 cholangiocyte cells were seeded on a 96-well plate and incubated for 24 hours with a standard growth medium. After removal of the standard medium, the cells were incubated with 200 μL of Dulbecco's modified Eagle's medium/F-12 (Gibco) contain-

ing premixed siRNA (10 nmol/L) and 0.75 μL of HiPerFect transfection reagent for 48 hours. Gene silencing was monitored using RT-PCR at the mRNA level and using immunofluorescence confocal microscopy at the protein level. Transfected cells were treated with LPS (0.5 μg/mL) for 48 hours. Cell proliferative activity was determined using the WST-1 assay.

Immunohistochemistry

The antibodies used were anti-VEGF antibody for rat (1:100, mouse monoclonal) from Abcam and anti-VEGF antibody for human (1:200, rabbit polyclonal), anti-CD31 antibody (1:100, rabbit polyclonal), anti-Flk-1 antibody (1:100, mouse monoclonal), anti-Flt-1 antibody (1:100, rabbit polyclonal), and anti-TLR4 antibody (1:100, rabbit polyclonal) from Santa Cruz Biotechnology (Santa Cruz, CA). After deparaffinization of the sections, antigen retrieval was performed by microwaving in 10 mmol/L citrate buffer pH 6.0. After blocking endogenous peroxidase, sections were incubated overnight at 4°C with individual primary antibodies. The sections were then incubated with secondary antibody conjugated to the EnVision+ system (DakoCytomation). Color development was performed using DAB, and the sections were counterstained with hematoxylin. For immunostaining of rat liver sections with anti-CD31 antibody, protein expression was detected using an alkaline phosphatase-labeled polymer (HISTOFINE system; Nichirei, Tokyo, Japan); color development was performed using a Vector Red alkaline phosphatase substrate kit (Vector Laboratories, Burlingame, CA). Control sections were evaluated by substitution of the primary antibodies with nonimmunized serum, resulting in no signal detection.

Microvessel Density

Liver sections stained with the anti-CD31 antibody were analyzed. The number of microvessels around the bile ducts was counted for five randomly selected fields in each section at ×400 magnification, and the value was defined as microvessel density.

Statistical Analysis

The mean ± SD was calculated for all parameters. Statistical differences were determined using *t*-test and analysis of variance. A P value of <0.05 was accepted as the level of statistical significance.

Results

Portal Neovascularization and Cholangitis in the PCK Liver

Portal neovascularization was examined using immunostained liver sections of 3-week-old, 2-month-old, and 10-month-old rats with anti-CD31 antibody. In normal rats of any age, vascular structures in the portal tract are composed mainly of portal vein, hepatic artery, and peribiliary vascular plexus; other vascular structures were unremarkable (Figure 1A). By contrast, portal neovascularization was evident in the PCK rats, and it tended to be increased in the aged rat (10-month-old; Figure 1A). Microvessel density was significantly higher in the PCK rats, compared with that of normal rats at any age examined; it reached the highest level in 10-month-old PCK rats (Figure 1B).

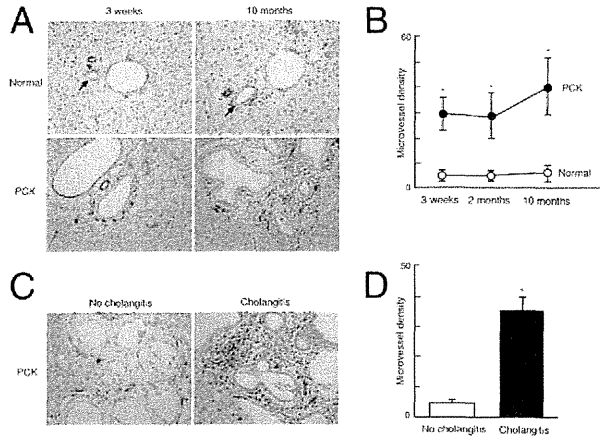

Figure 1. Portal neovascularization and cholangitis in the PCK liver. **A:** Vascular structures were visualized by immunohistochemical staining with anti-CD31. **B:** Microvessel density was significantly higher in the PCK liver, compared with that of normal rats; the value was highest in 10-month-old PCK liver. **C** and **D:** In 10-month-old PCK liver, portal neovascularization tended to be more densely seen at the sites of cholangitis, compared with sites of no cholangitis (**C**); analysis of microvessel density confirmed this tendency (**D**). **Arrows** indicate interlobular bile ducts of normal rats. $^*P <$ 0.01. Original magnification, ×400.

Chronic and/or suppurative cholangitis due to biliary infection became frequent histological findings in the PCK rats during aging. Cholangitis was rare in 3-week-old PCK rats, but it was frequently observed in the 10-month-old PCK rats. In 10-month-old PCK rats, portal neovascularization was more dense at the sites of cholangitis, compared with sites without cholangitis (Figure 1, C and D), suggesting a close correlation between portal neovascularization and biliary infection.

Expression of VEGF and Its Receptors in the PCK Liver

Immunohistochemical expression of VEGF was examined using liver sections of 3-week-old, 2-month-old, and 10-month-old rats. In normal rats, weak expression of VEGF was observed in the bile duct epithelium, and hepatocytes also showed diffuse and weak positive signals of VEGF (Figure 2A). More intense expression of VEGF was observed in the bile duct epithelium of PCK rats, and such staining tended to increase with aging (Figure 2A). In PCK rats, VEGF expression of the bile duct epithelium was not uniform in a single section; in some parts, the immunohistochemical labeling of VEGF of the bile duct epithelium was accentuated at sites of intense cholangitis, relative to sites of less inflammatory cell infiltrates (Figure 2B).

Immunohistochemical analysis showed that the bile duct epithelium constitutively expressed the VEGF receptors Flk-1 and Flt-1, in both normal and PCK rats (Figure 2C). The extent of immunohistochemical expression of

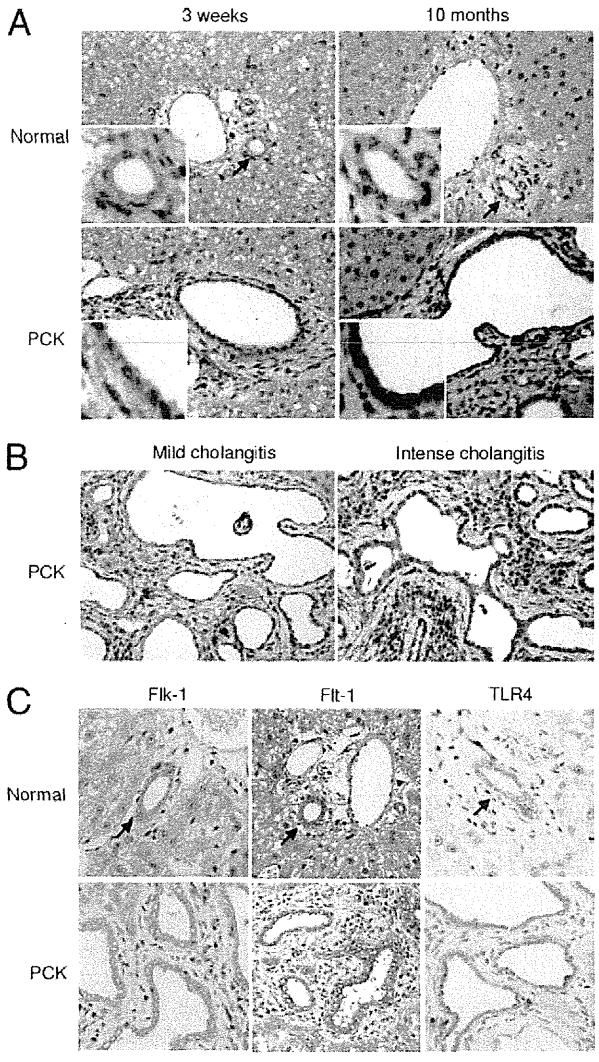

Figure 2. Expression of VEGF and its receptors in the PCK liver. **A:** The immunohistochemical expression of VEGF was more intensely observed in the bile duct epithelium of the PCK rats than in that of normal rats, and such staining tended to be increased along with aging of the PCK rats. **B:** In the PCK liver of 10-month-old age, there were foci in which the immunohistochemical labeling of VEGF of the bile duct epithelium was accentuated at the sites of intense cholangitis. **C:** Immunohistochemical analysis showed that the bile duct epithelium expressed the VEGF receptors Flk-1 and Flt-1 in both normal and PCK rats. The LPS receptor TLR4 was also expressed in the bile duct epithelium of both rats, and expression tended to be more intense in the PCK rats. **Arrows** indicate interlobular bile ducts of normal rats. Original magnification: ×400, main images; ×1000, insets.

Flk-1 and Flt-1 in the bile duct epithelium appeared to be similar between normal and PCK rats. The LPS receptor, TLR4, was also expressed in the bile duct epithelium of both normal and PCK rats, with a tendency toward more intense expression in the PCK rats (Figure 2C).

Portal Neovascularization and VEGF Expression in the Liver of Caroli's Disease

Around the intrahepatic bile ducts of Caroli's disease, the microvessels examined using liver sections immunostained with CD31 antibody were well developed (Figure 3A). The analysis of microvessel density confirmed this tendency (Figure 3B). The immunohistochemical expression of VEGF of the bile duct epithelium appeared to be increased in Caroli's disease, compared with that of normal liver (Figure 3C).

The bile duct epithelium was positive for immunohistochemical expression of Flk-1 and Flt-1, and expression was more intense in several cases of Caroli's disease, relative to that of normal liver, which is consistent with previous report.[14] In both normal liver and in Caroli's

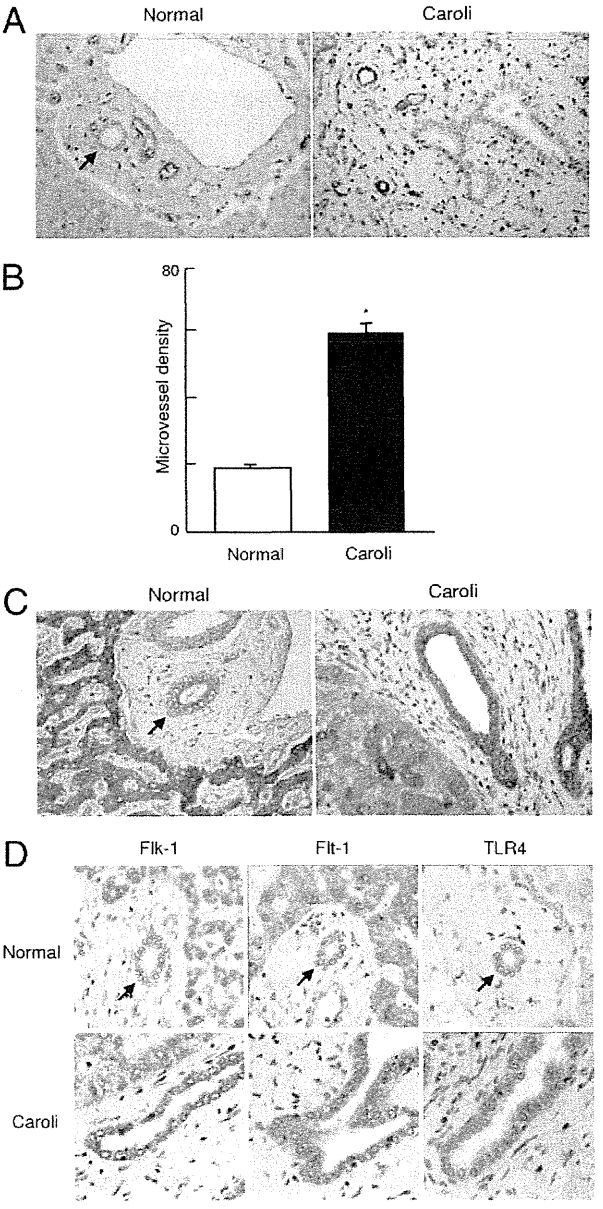

Figure 3. Portal neovascularization and VEGF expression in liver in Caroli's disease. **A:** Similar to findings from PCK rats, the microvessels were well developed around the intrahepatic bile ducts in human Caroli's disease, as examined using liver sections immunostained with CD31 antibody. **B:** Microvessel density was significantly higher in liver of Caroli's disease, compared with normal liver. **C:** Immunohistochemical expression of VEGF of the bile ducts appeared to be increased in liver of Caroli's disease. **D:** The bile duct epithelium was positive for immunohistochemical expression of Flk-1, Flt-1, and TLR4 in normal liver and in Caroli's disease; their expression tended to be more intense in liver of Caroli's disease. **Arrows** indicate interlobular bile ducts of normal liver. $^{*}P < 0.01$. Original magnification, ×400.

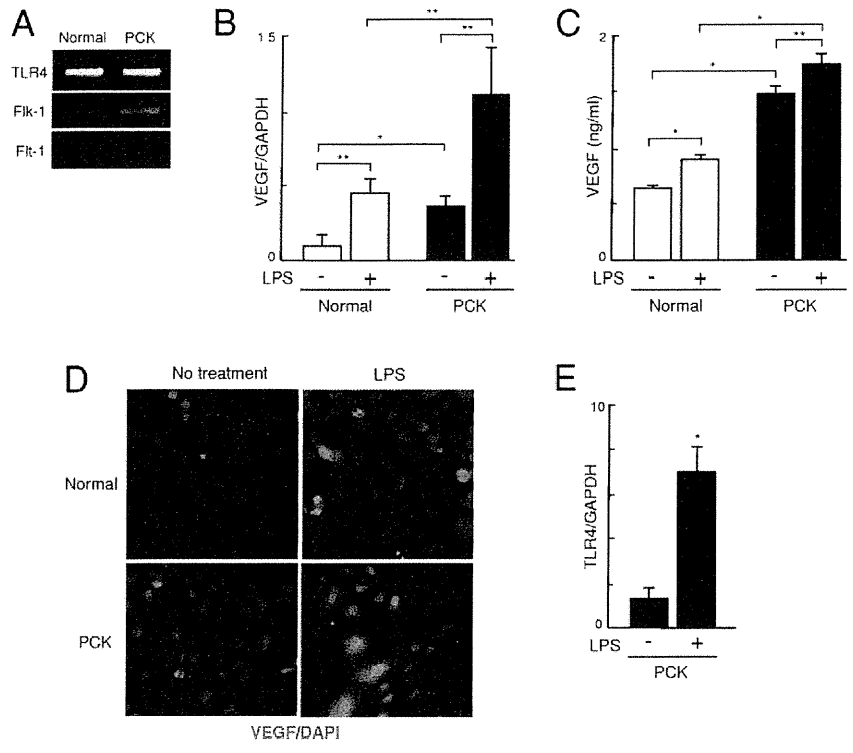

Figure 4. VEGF expression and effects of LPS on its expression of PCK cholangiocytes. **A:** Cholangiocytes were treated with LPS (10 μg/mL), and expression of VEGF was examined. RT-PCR analysis confirmed that cholangiocytes expressed TLR4 as well as Flk-1 and Flt-1. **B:** Real-time quantitative PCR analysis showed that PCK cholangiocytes initially overexpressed VEGF mRNA, and LPS significantly induced VEGF mRNA expression in both normal and PCK cholangiocytes at 3 hours after stimulation. **C:** ELISA analysis showed that the culture supernatant of PCK cholangiocytes contained a significantly high level of VEGF protein, and treatment with LPS for 24 hours further increased the VEGF level in the culture supernatant of both normal and PCK cholangiocytes. **D:** Immunofluorescence confocal microscopy also showed that LPS induced VEGF protein expression in both cell lines at 24 hours after LPS stimulation. **E:** LPS was also able to induce the expression of TLR4 mRNA of PCK cholangiocytes. $^{*}P < 0.01$; $^{**}P < 0.05$. Original magnification, ×1000.

disease, TLR4 was expressed in bile duct epithelium; more intense immunohistochemical labeling was observed in liver of Caroli's disease (Figure 3D). These results were almost identical to those for PCK rats, except for immunohistochemical expression of Flk-1 and Flt-1, suggesting that pathogenesis might be similar in the rodent model and in human disease.

VEGF Expression and Effects of LPS on Its Expression in PCK Cholangiocytes

To examine the angiogenic effects of PCK cholangiocytes in association with biliary infection, cultured cholangiocytes were treated with LPS, and the expression of VEGF was examined. RT-PCR analysis confirmed that the cholangiocytes expressed TLR4, as well as Flk-1 and Flt-1 (Figure 4A). Even in the absence of LPS stimulation, PCK cholangiocytes expressed a significantly high level of VEGF mRNA, and LPS further induced the expression of VEGF mRNA in cholangiocytes (Figure 4B).

The ELISA analysis showed that the culture supernatant of PCK cholangiocytes contained significantly high levels of VEGF protein, and that treatment with LPS further increased the VEGF level in the culture supernatant of both normal and PCK cholangiocytes (Figure 4C). Consistent with these findings, analysis using immunofluorescence confocal microscopy showed that LPS induced VEGF expression in both cell lines (Figure 4D).

In addition to the effects on VEGF induction in cholangiocytes, LPS was able to induce the expression of TLR4 mRNA in PCK cholangiocytes (Figure 4E).

Effect of LPS and VEGF on Cell Proliferation in PCK Cholangiocytes

Cell proliferative activity was determined at 24, 72, and 120 hours after stimulation with LPS and VEGF, using the WST-1 assay. At 72 hours after LPS stimulation, cell proliferative activity was significantly higher in PCK cholangiocytes, compared with that of the untreated groups (Figure 5A). In both normal and PCK cholangiocytes, LPS significantly induced cell proliferative activity at 120 hours after stimulation (Figure 5A).

VEGF also significantly increased cell proliferative activity of PCK cholangiocytes at 72 and 120 hours after stimulation, but cell proliferative activity was not increased in normal cholangiocytes at the concentrations of VEGF tested (Figure 5B).

To determine the effects of VEGF on cell proliferative activity, siRNA against VEGF was used. siRNA reduced VEGF mRNA and protein expression of the cholangiocytes, although their expression was not completely diminished (Figure 5C). As expected, cell proliferative activity of PCK cholangiocytes was significantly inhibited by VEGF siRNA (Figure 5D). The effects of VEGF on the induction of cell proliferative activity was further confirmed by studies using an inhibitor of VEGF receptor tyrosine kinase, SU5614 (Figure 5E).

Angiogenic Effects of PCK Cholangiocytes

The culture supernatant of PCK cholangiocytes contained significantly high levels of VEGF (Figure 4C). To further address the angiogenic effects of PCK cholangiocytes, the

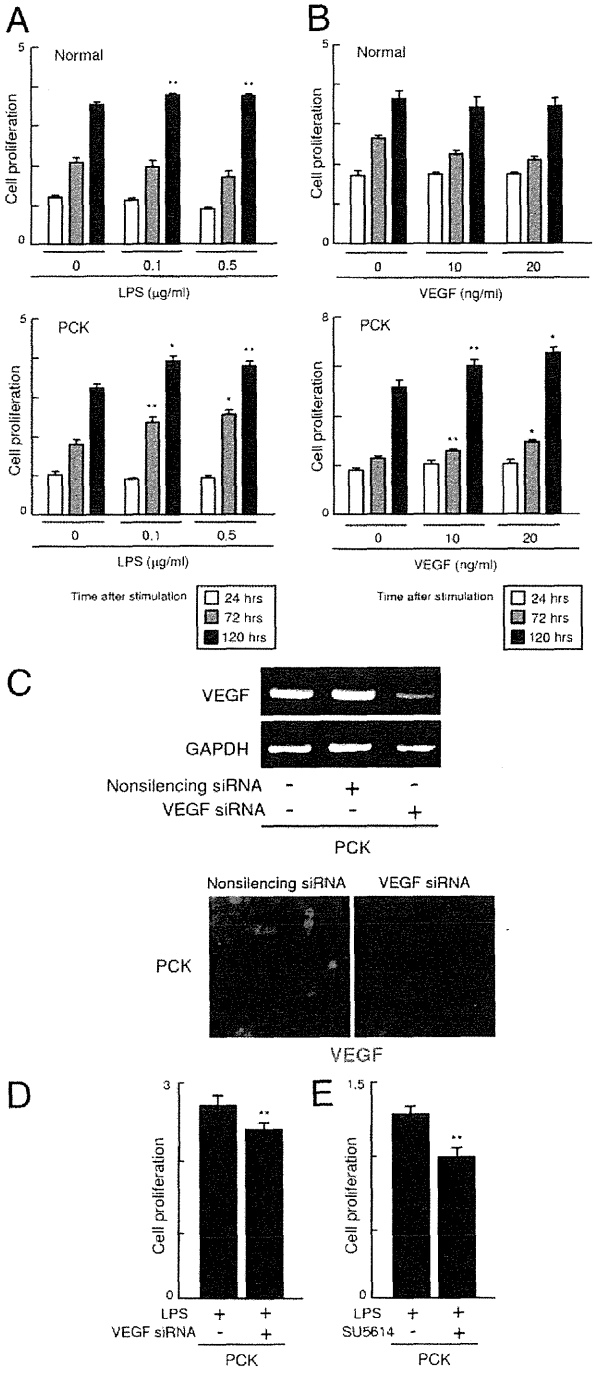

Figure 5. Effect of LPS and VEGF on cell proliferation of PCK cholangiocytes. **A:** Normal and PCK cholangiocytes were treated with LPS and VEGF at the concentrations indicated, and cell proliferative activity was determined using the WST-1 assay. In both normal and PCK cholangiocytes, LPS significantly induced cell proliferative activity of PCK cholangiocytes at 72 hours after stimulation, and it was significantly increased in both normal and PCK cholangiocytes at 120 hours. **B:** VEGF significantly increased cell proliferative activity of PCK cholangiocytes at 72 and 120 hours after stimulation, but did not affect cell proliferation in normal cholangiocytes at the concentrations of VEGF tested. **C:** VEGF siRNA reduced the expression of VEGF mRNA and VEGF protein in PCK cholangiocytes, which was evaluated using RT-PCR and immunofluorescence confocal microscopy, respectively. **D:** Cell proliferative activity was significantly inhibited by treatment with VEGF siRNA at 48 hours after LPS treatment. **E:** Treatment of PCK cholangiocytes with the VEGF receptor tyrosine kinase inhibitor SU5614 also significantly reduced cell proliferative activity at 48 hours after LPS treatment. $^{*}P < 0.01$; $^{**}P < 0.05$ versus untreated experimental groups at the same time period after stimulation (**A** and **B**); $^{**}P < 0.05$ versus untreated experimental groups with VEGF siRNA (**D**) and SU5614 (**E**). Original magnification, ×1000 (**C**).

culture supernatant of cholangiocytes of normal and PCK rats was added to the dishes in which RAOECs were cultured, and the cell proliferative activity of the RAOECs was determined. Both normal and PCK culture supernatant significantly induced cell proliferative activity of RAOECs, compared with that of the basal medium only; the culture supernatant of PCK cholangiocytes had more prominent effects on the induction of cell proliferative activity, compared with normal cholangiocyte supernatant (Figure 6A).

The tube formation assay using RAOECs demonstrated that the addition of PCK cholangiocyte culture supernatant induced the branching pattern of growth of RAOECs (Figure 6B), and the quantitative analysis of the number of branching points showed that the PCK cholangiocyte culture supernatant significantly increased this pattern, compared with the normal supernatant (Figure 6C). Notably, the treatment of RAOECs with the cholangiocyte culture supernatant obtained after 24-hour LPS treatment further accelerated the branching of RAOECs (Figure 6, B and C).

In the analysis using a cell migration chamber, the addition of cholangiocyte culture supernatant significantly increased cell migration activity of RAOECs; the PCK culture supernatant had more prominent effects than the normal supernatant (Figure 6D). Again, the addition of LPS-treated cholangiocyte culture supernatant further increased the migration activity of RAOECs (Figure 6D).

Cell Signaling Pathways Involved in VEGF Expression in PCK Cholangiocytes

In both normal and PCK cholangiocytes, LPS induced NF-κB activation (Figure 7A). Under immunofluorescence confocal microscopy, nuclear expression of NF-κB p50 and p65 was observed in both cell lines after LPS stimulation, and the NF-κB inhibitor isohelenin inhibited nuclear translocation of NF-κB p50 and p65 (Figure 7B). Despite inactivation of NF-κB by isohelenin, the expression of VEGF induced by LPS was unaffected (Figure 7C).

Western blot analysis showed that LPS induced phosphorylation of Akt and JNK/SAPK in both cholangiocyte cell lines (Figure 7D), but phosphorylation of ERK1/2 and p38 MAPK was unaffected (data not shown). The increased phosphorylation of Akt was observed in PCK cholangiocytes even in the absence of LPS stimulation (Figure 7D). The PI3K inhibitor LY294002 reduced the expression of VEGF after LPS stimulation in PCK cholangiocytes (Figure 7E). JNK inhibitor I and JNK inhibitor II also significantly reduced the LPS-induced VEGF expression in PCK cholangiocytes (Figure 7F), demonstrating the involvement of PI3K-Akt and JNK pathways in the induction of VEGF by LPS.

Discussion

In the present study, we elucidated the pathogenic significance of biliary infection in the progression of cystic dilation of the intrahepatic bile ducts in PCK rats. Microvessels around intrahepatic bile ducts were well developed in PCK rats, and this vascular development